NUMERICAL ANALYSIS OF EFFECTS OF THE TWISTING ANGLE ON THERMOHYDRAULIC PERFORMANCE OF A HEXAGONAL PIN FIN ARRAY

2022
MASTER THESIS
MECHANICAL ENGINEERING

Noora Imad ALGBOURIE

Thesis Advisor
Prof. Dr. Kamil ARSLAN

NUMERICAL ANALYSIS OF EFFECTS OF THE TWISTING ANGLE ON THERMOHYDRAULIC PERFORMANCE OF A HEXAGONAL PIN FIN ARRAY

Noora Imad ALGBOURIE

T.C.
Karabük University
Institute of Graduate Programs
Department of Mechanical Engineering
Prepared as
Master Thesis

Thesis Advisor
Prof. Dr. Kamil ARSLAN

KARABÜK
June 2022

I certify that in my opinion the thesis submitted by Noora Imad ALGBOURIE titled "NUMERICAL ANALYSIS OF EFFECTS OF THE TWISTING ANGLE ON THERMOHYDRAULIC PERFORMANCE OF A HEXAGONAL PIN FIN ARRAY" is fully adequate in scope and in quality as a thesis for the degree of Master of Science.

Prof. Dr. Kamil ARSLAN .....
Thesis Advisor, Department of Mechanical Engineering

This thesis is accepted by the examining committee with a unanimous vote in the Department of Mechanical Engineering as a Master of Science thesis. June 17, 2022

Examining Committee Members (Institutions)	Signature
Chairman : Assoc. Prof. Dr. Engin GEDİK (KBU)	.....
Member : Prof. Dr. Kamil ARSLAN (KBU)	.....
Member : Assist. Prof. Dr. Hüseyin KAYA (BU)	.....

The degree of Master of Science by the thesis submitted is approved by the Administrative Board of the Institute of Graduate Programs, Karabük University.

Prof. Dr. Hasan SOLMAZ .....
Director of the Institute of Graduate Programs

"I declare that all the information within this thesis has been gathered and presented in accordance with academic regulations and ethical principles and I have according to the requirements of these regulations and principles cited all those which do not originate in this work as well."

Noora Imad ALGBOURIE

ABSTRACT

M.Sc. Thesis

NUMERICAL ANALYSIS OF EFFECTS OF THE TWISTING ANGLE ON THERMOHYDRAULIC PERFORMANCE OF A HEXAGONAL PIN FIN ARRAY

Noora Imad ALGBOURIE

Karabük University
Institute of Graduate Programs
Department of Mechanical Engineering

Thesis Advisor:
Prof. Dr. Kamil ARSLAN
June 2022, 70 pages

In this study, the effects of pitch ratio and diagonal length of twisted pin fin array in heat sink on the flow and heat transfer characteristics have been determined numerically. Numerical calculations have been conducted under turbulent flow condition ($2658 \leq Re \leq 7138$). While the length of edge has been changed $3 \leq L_{ef} \leq 6$ and the pitch ratio has also been varied between $0.75 \leq p/e \leq 1.1$. Variation of twisting ratio (TR=50, 100, 200) of the pin fins has also been examined in detail.

The study has been carried out using Ansys Fluent 2020R2 code with low-Re correction application and SST k-ω turbulence model. Using numerical results, to reveal the flow characteristics comprehensively, the contours have been created for vorticity, velocity, and temperature. The thermohydraulic performance of the study has been clarified in detail with calculating average Nusselt number, average Darcy

friction factors, thermal resistance, and Performance Elevation Criteria (PEC). In the first part of this thesis, heat exchangers and heat sinks are explained in detail. Especially, types and designs of heat sinks, the principals of heat transfer and the thermal resistance concept have been defined in detail. The fin arrangements and the mechanism of action of the fins in heat sinks have also been presented.

In the second part of the thesis, the research and studies that were conducted previously in this field and the developments that occurred in them are discussed in detail.

In the third part of the thesis, numerical method is presented in detail. Governing equations with boundary conditions are given. Numerical procedure is also defined in detail in this section.

In the fourth part of the thesis, the results have been given with graphs and contours for different cases. The case1 for TR=50 has been determined as the optimum case for this study.

In the Conclusion section of the thesis all the findings have been given in briefly.

Key Words : Pin fin, heat sink, twisting ratio, convection heat transfer, CFD.
Science Code : 91411

ÖZET

Yüksek Lisans Tezi

BURULMA AÇISININ BİR ALTIGEN PİM DİZİSİNİN TERMOHİDROLİK PERFORMANSI ÜZERİNDEKİ ETKİLERİNİN SAYISAL ANALİZİ

Noora Imad ALGBOURIE

Karabük Üniversitesi
Lisansüstü Eğitim Enstitüsü
Makine Mühendisliği Anabilim Dalı

Tez Danışmanı:
Prof. Dr. Kamil ARSLAN
Haziran 2022, 70 sayfa

Bu çalışmada, ısı alıcıdaki bükümlü pin kanat dizisinin hatve oranı ve diyagonal uzunluğunun akış ve ısı transfer özellikleri üzerindeki etkileri sayısal olarak belirlenmiştir. Türbülanslı akış koşulunda ($2658 \leq Re \leq 7138$) sayısal hesaplamalar yapılmıştır. Kenar uzunluğu $3 \leq L_{ef} \leq 6$ aralığında değiştirilirken, hatve oranı ise $0.75 \leq p/e \leq 1.1$ arasında değiştirilmiştir. Pim kanatlarının burulma oranının (TR=50, 100, 200) değişimi de detaylı olarak incelenmiştir.

Çalışma, SST k-ω türbülans modeli ve düşük Re düzeltme uygulaması ile Ansys Fluent 2020R2 kodu kullanılarak gerçekleştirilmiştir. Akış özelliklerini kapsamlı bir şekilde ortaya çıkarmak için sayısal sonuçlar kullanılarak girdap, hız ve sıcaklık için kontür grafikler oluşturulmuştur. Çalışmanın termohidrolik performansı, ortalama Nusselt sayısı, ortalama Darcy sürtünme faktörleri, termal direnç ve Performans Değerlendirme Katsayısı (PDK) hesaplanarak detaylı olarak sunulmuştur.

Tezin ilk bölümünde, ısı eşanjörleri ve ısı alıcıları detaylı olarak açıklanmıştır. Özellikle, ısı alıcı çeşitleri ve tasarımları, ısı transferinin esasları ve ısıl direnç kavramı ayrıntılı olarak tanımlanmıştır. Ayrıca, ısı alıcılardaki kanatçık düzenlemeleri ve kanatçıkların etki mekanizması da sunulmuştur.

Tezin ikinci bölümünde, bu alanda daha önce yapılmış araştırma ve çalışmalar ile bunlarda meydana gelen gelişmeler ayrıntılı olarak ele alınmıştır.

Tezin üçüncü bölümünde, sayısal yöntem ayrıntılı olarak sunulmuştur. Temel denklemler ve sınır koşulları verilmiştir. Sayısal çözüm yöntemi bu bölümde ayrıntılı olarak tanımlanmıştır.

Tezin dördüncü bölümünde, farklı durumlar için sonuçlar grafikler ve kontürler ile sunulmuştur. *TR*=50 için Durum1 koşulu bu çalışma için optimum durum olarak belirlenmiştir.

Tezin Sonuç bölümünde ise tüm bulgular kısaca özetlenmiştir.

Anahtar Kelimeler : Pin kanatçık, soğutucu , büküm oranı, taşınım ile ısı transferi, HAD.

Bilim Kodu : 91411

ACKNOWLEDGMENT

In the beginning, I would like to present my great thanks to my supervisor Prof. Dr. Kamil ARSLAN for all the information and acknowledgment that I got from him and for his support, understanding, and unlimited kindness. I'm really happy and grateful that I had the chance to be his student. Also, I would like to thank my family for their support. Especially my mum, thank you for always being there for me I would never do this without you. This achievement is dedicated to you. And finally, thanks to my friend MSc. student Hayati Kadir PAZARLIOĞLU for his help.

CONTENTS

Page

Page

LIST OF FIGURES

Page

Page

Page

LIST OF TABLES

Page

SYMBOLS AND ABBREVITIONS INDEX

SYMBOLS

A : area, m^2

D : diameter, m

e : distance between the fins in streamwise direction, m

f : friction factor, -

F_L : fins length, m

H : height, m

H : heat transfer coefficient, $W/m^2.K$

k : thermal conductivity, W/m.K

Kc_p : specific heat at constant pressure, J/kg.K

L : length, m

L_{ef} : diagonal length of the pin fins, m

L_d : length of the rectangular duct, m

$\dot{m}$: mass flow rate, kg/s

Nu : Nusselt number, -

p : pressure, Pa

p : distance between the fins in spanwise direction, m

PEC : Performance Elevation Criteria, -

$\dot{Q}$: heat transfer rate, W

R : thermal resistance, K/W

T : Temperature,K

TR : twisting ratio, -

u : velocity, m/s

W : width, m

W_d : dimension of inlet and outlet section of the rectangular duct, m

$W\theta$: twisting angle, degree

σ : Stefan-Boltzmann constant, $5.67\times 10^{-8} W/m^2.K^4$

ρ : fluid density, kg/m^3

δ : thickness, m

η : efficiency, -

PART 1

INTRODUCTION

1.1. HEAT EXCHANGERS

In our time, it has become necessary to provide effective cooling mechanisms to avoid an excessive rise in the temperature of electronic components. As most electronic systems require heat exchangers to maintain operating temperature. Forced air cooling technology is one of the most effective methods for thermal management and cooling of electronic equipment in a traditional-sized heat sink. The size of heat exchangers is determined according to the limited space in which they will be installed. So, they must be installed with taking in account the low pressure and available space as well as thermal performance. Hence, the importance of numerical improvement in heat exchanger design has been gradually emphasized [1]. In Figure 1.1, an example of photography of heat exchanger is given.

Figure 1.1. An example photograpy of heat exchanger [2].

The heat exchanger concept was conceived in the 1970's to eliminate the destructive tube vibrations caused by the flux found in conventional plate heat exchangers where the ROD BAFFLE design was used. As this early exchangers showed a low loss in shell pressure and an increase in thermal performance [3]. Where it was found that the ideal heat exchanger contains the same UA and the same arithmetic mean temperature difference, which makes the heat exchanger less reversible and more efficient that it transfers the maximum amount of heat equal to the product of UA and the arithmetic average of the temperature difference and generates the minimum entropy. Heat exchanger efficiency is defined as the ratio of heat transferred in the actual heat exchanger to the heat that will be transferred in the ideal one [4]. It has also become necessary to reduce the cost of heat exchangers due to the widespread use of them in industrial processes. In the traditional design approaches, iterative procedures were resorted, so the design criteria were gradually changed to reach a satisfactory solution that meets the specifications required for the design. But these methods usually take long time to reach the economically optimal solution [5]. The evaluation of the performance of electronic devices, especially high-power devices, depends on the management of thermal technology, and this is consistent with the rapid development witnessed by the world of integrated electronic circuit systems with high technical characteristics and small size [6]. High temperatures resulting from the high thermal effect of high operation cause damage to the most of electronic devices [7].

1.1.1. Types Of Heat Exchangers

Heat exchangers has been classified to four main types [8]:

a) *Double Pipe Heat Exchanger:* Basically, made of two different diameters tubes inserted in each other. The pipes all parts are assembled into coil by using clutch coupling that provides the required space for cooling and heating. The flow is towards each other directly while the sections are placed one above the other (Figure 1.2).

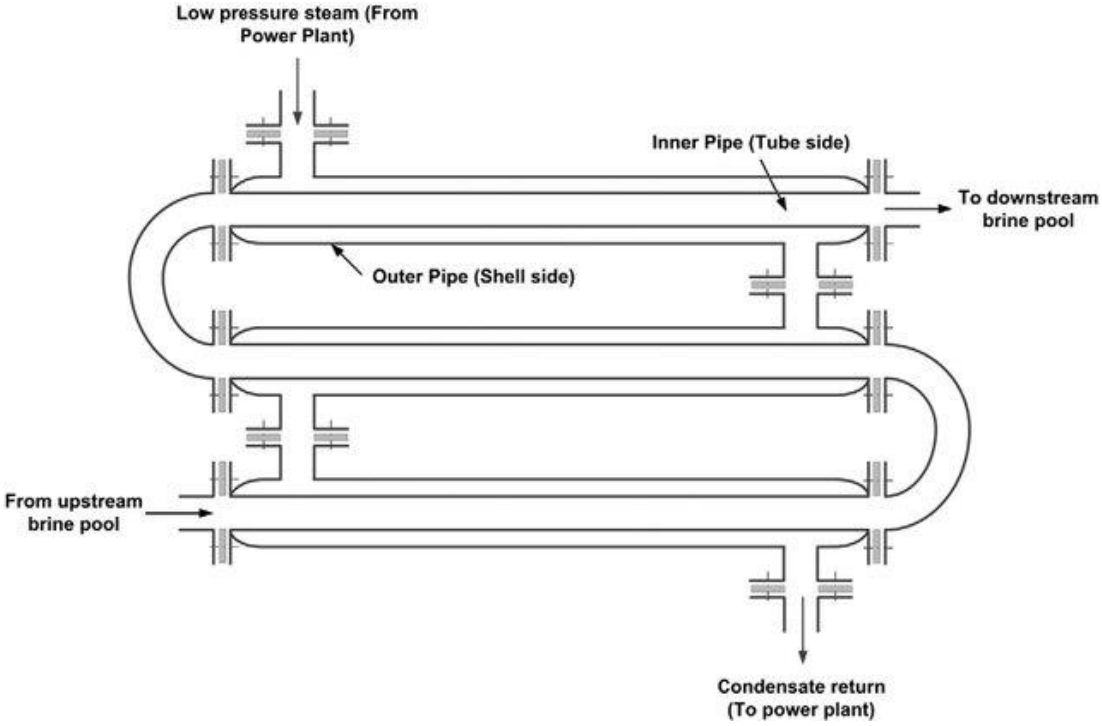

Figure 1.2. Double pipe heat exchanger [9].

b) *Shell* and *Tube Heat Exchangers:* It consists of two main parts, an integrated tubing section and a tubular tank. The heat carriers are directed in the heat exchanger both towards each other and parallel (Figure 1.3).

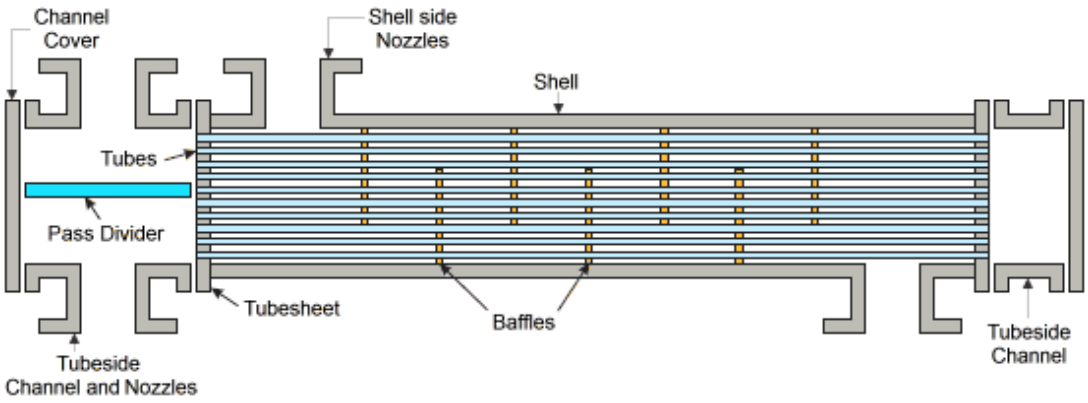

Figure 1.3. Shell and tube heat exchanger [10].

c) *Plate Heat Exchangers:* This type of heat exchangers are made of number of plates separated from each other by using seals that installed without the use of any adhesive mixtures. These plates are made from stainless steel (Figure 1.4).

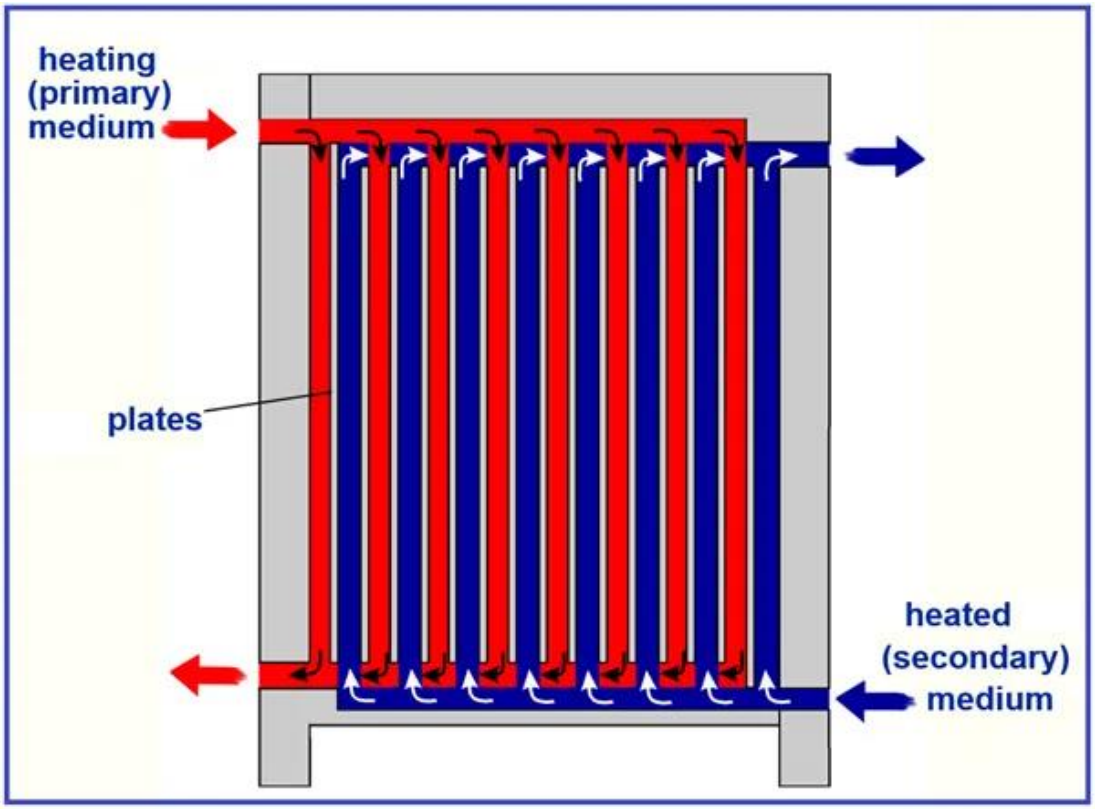

Figure 1.4. Plate heat exchanger [11].

d) *Spiral Plate Heat Exchanger:* These type of heat exchangers consist of two metal plates which are wonded to each othere one of the proceses treams enters from outside and flowes inword and the second stream interes the heat exchanger throw the center and flows from the outside (Figure 1.4).

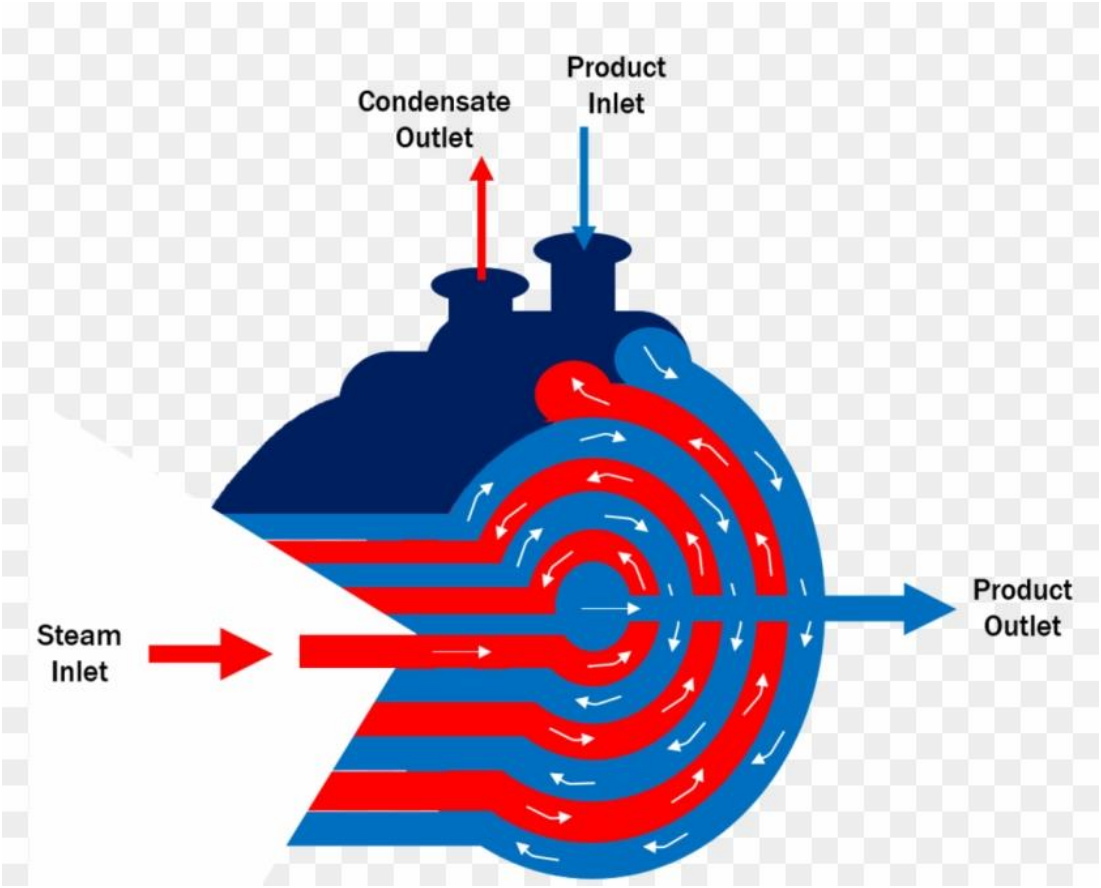

Figure 1.5. Spiral plate heat exchanger [11].

1.2. HEAT SINK

Heat sink is the name that called on the substance or the device that absorbs or dissipates especially unwanted heat one of the most popular cooling technologies in electronics systems. An example for a heat sink is presented in Figure 1.6.

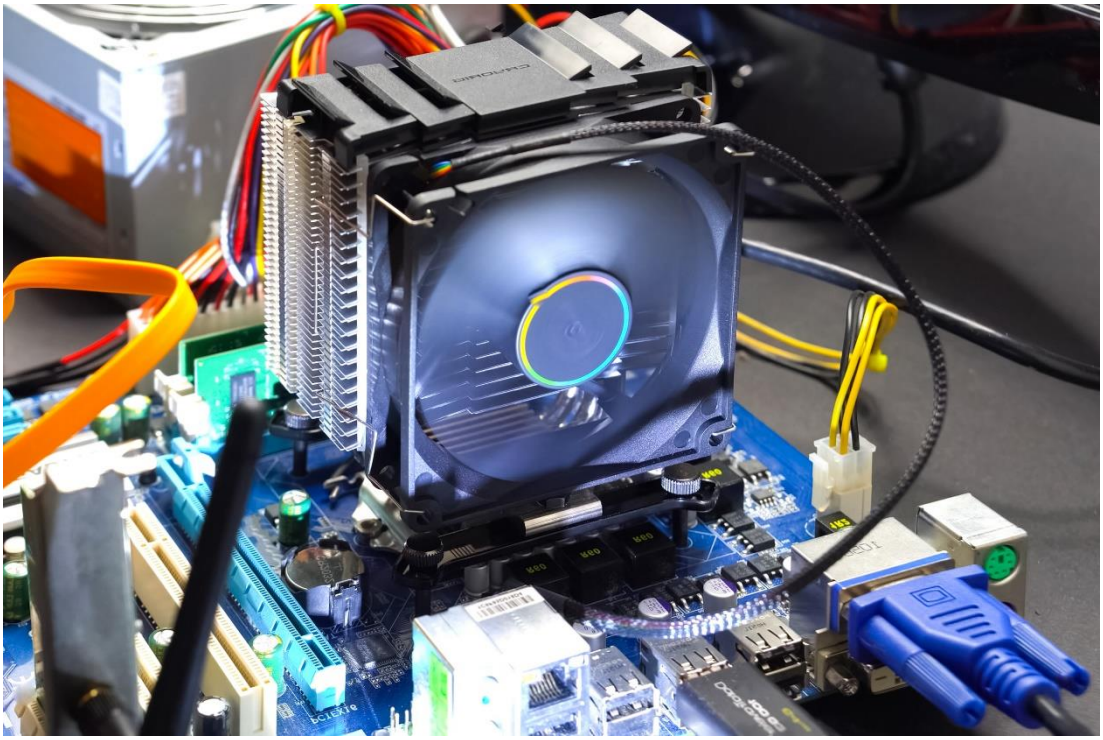

Figure 1.6. Cooling electronics using heat sink [12].

Heat sinks are used to dissipate excess thermal energy. Most of the time they are made of aluminum and copper, but due to the higher prices of copper, they are little used. The heat sink is part of an integrated cooling system where it is combined with Pelletier cells or with heat pipes. When the performance of the heat sink is insufficient, hybrid solutions are used, such as combining them with active cooling systems such as fans. Due to the low difference in temperature between the heat sink and ambient air, this requires the use of forced air circulation.

Heat sinks are characterized by no need for electrical energy, as well as silent operation, and they do not contain moving parts that can be damaged over time. Usually, the biggest defect is the insufficient cooling power in the case of highly heated sensitive elements, and this defect is avoided by sufficient air flow through the heat sink. In despite of considering this process as a solution to the previous defect, it has negatives. As it requires the introduction of fans and devices with a high degree of unreliability, the size of the heat sink must be large and therefore heavy to perform its function.

1.2.1. Choosing Heat Sink

The selection of the heat sink depends on calculations based on simple formulas derived from Ohm's law and requires knowledge of the wasted power. For both the refrigerant component and the heat sink to the ocean and are provided by the manufacturers of both components. The thermal resistance from state to heat, and it is estimated by knowing the number of insulating joints and the type of contact.

The calculation of the heat sink strength differs between the normal state (non-forced air flow) from the heat sink provided with cooling tubes or a fan. In the case of choosing the heat sink, consideration must be given to reduce the thermal resistance that can be reached as much as possible, with the resistance between the heat sink and the environment in the foreground. It must also be ensured the fastest flow that the coolant can reach, the largest surface area of the dispersion and the largest heat capacity of the coolant. Water has a much higher heat capacity than air, which provides the possibility of a larger temperature difference between the dispersant and coolant, and thus ensures a faster heat transfer. It must be taken into account not to ignore the basic parameters, such as the type of socket installation suitable for the heat sink and the dimensions of the heat sink commensurate with a fixed area, as well as reducing the noise level to the maximum extent possible.

1.2.2. Heat Sink Types and Designs

Heat sinks are categorized to make it easier to distinguish between them [13].

a) *Active Heat Sinks with Fan*: They contain a fan that provides forced air flow through the heat sink as it can be seen in Figure 1.7.

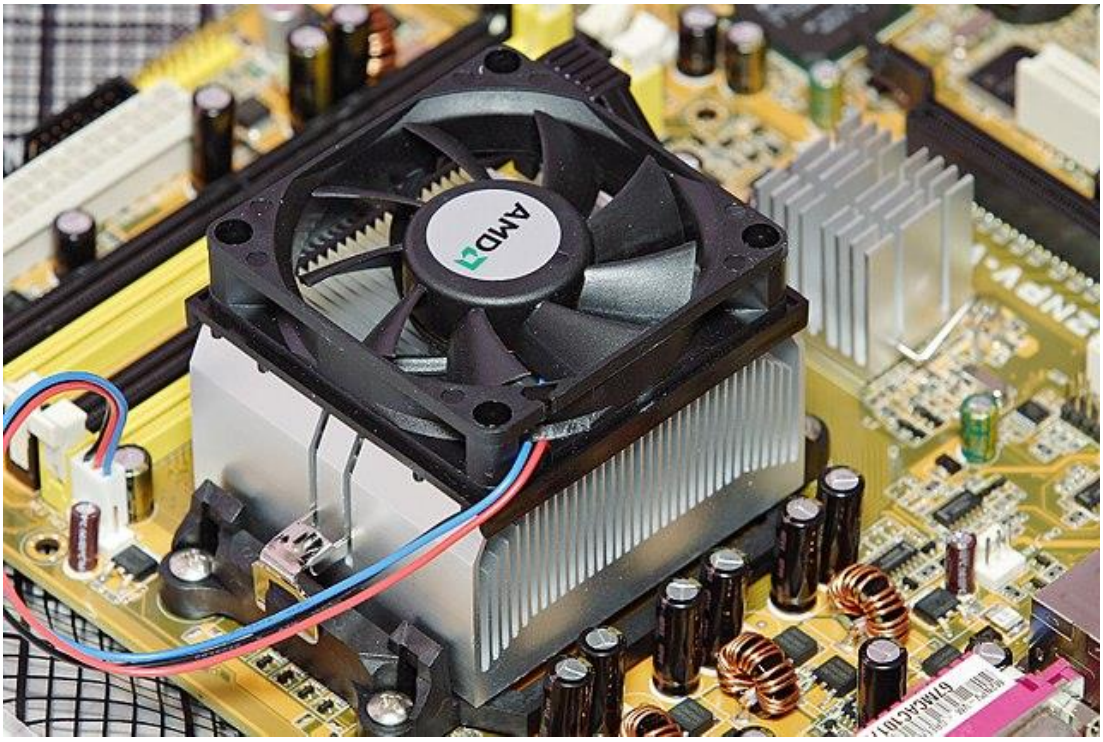

Figure 1.7. Heat sink with a fan [14].

b) *Active Heat Sinks with Heat Pipes:* It contains heat tubes that collect heat from the coolant component and then dissipate it to the fins and from there to the air. They are usually made of aluminum fins as given in Figure 1.8.

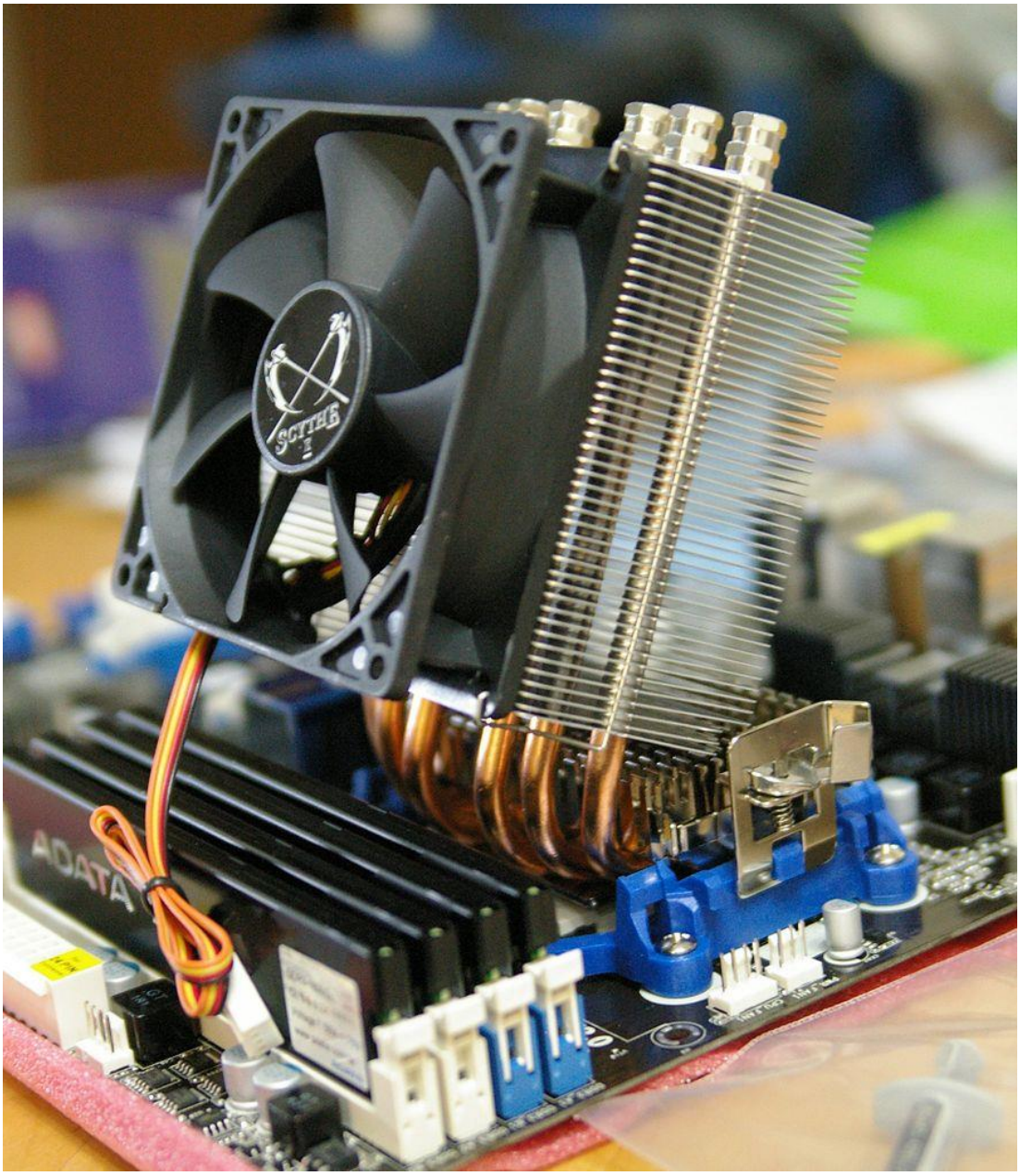

Figure 1.8. Heat sinks with heat pipes.

c) *Active Heat Sinks Equipped with Water Cooling:* The forced circulation of the liquid pump leads to heat dissipation mainly and is controlled by an expansion tank, this type is ideal for high power semiconductors. The heat sinks can also be divided, depending on their shape, into flat heat sinks, finned heat sinks, and U-type heat sinks. There are also many subspecies within these three categories. The great diversity in the forms of heat sinks results from the need to install them on different types of components, where their shape is modified

according to these components to provide the largest possible contact surface to improve the heat dissipation process as well as to simplify assembly. Where the heat sink is a transfer of thermal energy from a device with a high temperature to a fluid medium with a lower temperature. This medium is often air, but it can also be water or oil. The heat sink in the middle of the liquid water is called the cold plate in thermodynamics, where the heat sink acts as a thermal tank that absorbs a random amount of heat without a significant change in temperature. Heat sinks for electronic devices must have a temperature higher than the ambient temperature in order to transfer the heat by convection, radiation and conduction. The power sources for electronics are no longer fully efficient, so additional heat is produced, which is often harmful to the device.

1.2.3. Heat Transfer Principles in Heat Sink

In duct heat sink cases, the base of the heat sink is often hotter than the air flowing in the duct. Under steady state conditions and Newton's law of cooling, the application of energy conservation to the temperature contract gives the following equation:

$$Q^{\cdot} = m^{\cdot} C_{p,in}(T_{air,out} - T_{air,in}) \tag{1.1}$$

$$Q^{\cdot} = \frac{T_{hs} - T_{air,av}}{R_{hs}} \tag{1.2}$$

where

$$T_{air,av} = \frac{T_{air,in} + T_{air,out}}{2} \tag{1.3}$$

In the case of a relatively short heat sink, it is valid to use the average air temperature. By default, the logarithmic average of the air temperature is used when calculating the combined heat exchangers, which is a rate of air mass flow in kilograms/s. From the foregoing laws, it becomes clear to us that the average air temperature increases when its flow through the diffuser decreases, leading to an increase in the temperature of the

base of the diffuser and an increase in its thermal resistance, as the temperature of the base of the heat sink is strongly related to the temperature of the incoming air.

1.2.4. Thermal Resistance

The idea of thermal resistance simplifies the idea of choosing heat sinks in semiconductors used in a variety of consumer and industrial electronics. The heat flow is designed in the form of a series of resistance to the heat flow between the semiconductor mold and the surrounding air, so that the resistance from the mold to the device case is from the device case to the dispersion as well as from the diffuser to the air. The total resistance, the resistance from the mold to the surrounding air, is the sum of the aforementioned resistances. Thermal resistance is defined as the resulting rise in the temperature of each unit of energy and is expressed in units (℃/watts). The temperature rise of the mold above the surrounding air can be calculated if the total thermal resistance is calculated and the dispersion of the device in watts is known.

The idea of the thermal resistance of a semiconductor is an approximate idea, as it designs only a system in a state of non-equilibrium, taking into account the non-uniform distribution of heat on a device or heat sink, as well as the change in temperatures over time. With regard to temperature rise, it does not reflect the nonlinearity of radiation and convection. But for the purpose of simplifying the selection of commercially manufactured heat sinks, manufacturers tabulate typical values of the thermal resistance of semiconductor devices and heat sinks.

1.2.5. Fin Arrangements

A heat sink that has pin fins extending from its base is called a pin fin heat sink. These pins can be cylindrical, square, or hexagonal shapes. The pin is one of the most available and common types of heat sinks in the market, and the straight fin comes in second place in the arrangement of the heat sink fin, where the latter runs along the entire length of the heat sink. In finned heat sinks there is generally free convective flow around the heat sink, and it works better as the surface area of the heat sink

increases. The concept of a pin-fin heat sink is an attempt to collect as much surface area in each volume as possible.

1.2.6. The Mechanism of Action of the Fins

The heat sink fins provide a large surface for heat dissipation. The contact surface is the surface where the heat is transferred from the cooled component. So, this surface must be polished as smooth as possible to improve adhesion. Usually, silicone pastes are used to improve thermal conductivity and serve as heat sink insulators if necessary. Due to the benefit of convection heat sinks, many of them are placed vertically in special containers to achieve the best use of convection while providing an air outlet at the top and bottom, as this often eliminates the need for a fan as a result of increasing the air flow significantly because how much the heat sink's hotties increase. The air will pass faster through it to dissipate heat. The cooling performance depends on a large extent on the temperature difference between the diffuser and the environment. Although aluminum is a good conductor of heat, its performance is poor in the emissivity side, which requires covering the surface of aluminum heat sinks with an oxidized layer. Which is often one of the two colors black or blue, which increases its heat emission to a percentage that may reach 100%.

PART 2

LITERATURE REVIEW

In the last years, the machines were getting more and more complicated which led to the request for better cooling systems and working to get better heat dissipation in order to ignore the failure of the machine and give them a longer life and better performance.

As it known, the heat is removed by the active and passive cooling methods. The active method depends on the use of energy, unlike the passive cooling that does not use energy. Heat sink which is known as a passive heat exchanger that transfers the heat generated by an electronic or a mechanical device to a fluid medium is one of the popular thermal cooling technology for electronics [15,16]. Therefore, it is more appropriate in terms of cost, and does not contain moving parts, making it more reliable in many systems such as aircraft cooling engines, cooling electronic devices, air conditioners, refrigerator cooling engines, etc. [17]. The fins form an important component to improve and enhance the heat dissipation process of the heat sink diffuser [18]. The effect of temperature and humidity differences on the efficiency of the exponential species led to the analysis of the porous fin formations [19]. And the effect of installing the expansion or contraction mechanism on the surface of the fin helps to enhance the heat transfer and the efficiency of the longitudinal rectangular fin, indicating that the expansion degrades the efficiency while the shrinkage provides better efficiency [20]. In Turkyilmazoglu's investigation, it is important to obtain accurate formulas and results for the thermal efficiency and properties of the exponential fins in the heat sink [21].

Cooling media differs in heat sinks. It may be water, air or nanofluid. Several studies were conducted using water as a cooling medium, where three-dimensional numerical simulations were conducted to study the heat transfer and fluid flow characteristics in

a micro-channel design with sinusoidal cavities and rectangular ribs (*MC-SCRR*) combining two important features, a large flow area that significantly reduces high flow disturbances which occur due to the presence of ribs in the central part of the channel and reduce the pressure drop [22]. Vertical fin heat sinks were handled and numerically investigated for convective and radiation heat transfers by Mousavi [23]. Concluding that the L-shaped fins are characterized by the lowest temperature and no increase in weight, which makes them have the best performance compared to other designs. Heat sinks with five different distances between the fins (0.2, 0.5, 1, 1.5 mm) along with the flat plate heat sink were examined by Jajja et al. at the heat sink with a distance of 0.2 mm. The minimum base temperature was reached, which was 40.5 ^{o}C, explaining when the fin spacing is reduced and the volumetric flow rate of the water circulating through the heat sink is increased, the core temperature and thermal resistance of the heat sinks decrease [24]. The generation of a huge temperature in micro-electronic devices has become a result of the continuous development of modern electronics and communication technologies into compact and effective devices. The applicability of having a variable channel and variable width dual-layer heat sink was experimentally investigated in order to develop a test setup for the experimental investigation of the effect of variable heat flow [25]. To regulate the mass flow rate, heat responsive heat shrinkage hydrogels that provide more hot spots for cooling liquids are placed in nano heat sinks to solve the problem of chip failure that arises as a result of local hot spots [26]. Change the wavelength and amplitude along the flow direction of a nanochannel heat sink for the purpose of design optimization. The formation of vortices in the junction of the channel that occurs as a result of the curved walls is the reason for the improvement of heat transfer and which enhances the mixing of the coolant as well as enhances the convection of heat transfer between the walls of the channel and the coolant [27]. The use of corrugated heat sink with water-resistant walls instead of straight heat sink with small duct which have conventional walls is an effective method of cooling [28]. It also examined fluid flow and heat transfer behaviors in the presence of water as a cooling medium [29]. The heat transfer performance and the movement behavior of nanofluids in the sheath were studied inside an opposite T-shaped container containing porous media with different materials and structures, finding that at high values of Darcy's friction factors ratio and low values of parameter ratio in the solid state, the average Nusselt number has a

maximum value [30]. When Hartmann number increases to higher values of Rayleigh number, this leads to a decrease in the average Nusselt number, according to a study conducted by Mohsen Izadi for the transmission of heat radiation and thermal gravity of a microscopic nano-liquid in an anomalous chamber in the presence of a regular magnetic effect [31]. Considering the effect of micro-cycles on the thermal properties of the flow, the thermal energy transfer properties of the thermo gravity of a polar nano-chamber were analyzed. By the slope of the magnetic field depends entirely on the value of the conduction performance [32]. Many studies have also been conducted that deal with nanofluids as a cooling medium with different types and concentrations [33–37]. And the first law and second law of a hybrid performances have been evaluated by Shahsavar et al. [38]. By using the first and second low, a newly designed heat sink was made by Shahsavarb and Entezari to evaluate effects of the porous medium and water-silver biological nanofluid on the performance [39]. Yoon et al. conducted a research on the heat dissipation of heat sink by using air as a cooling medium to improve its performance to be more effective and efficient because it is one of the most popular cooling technologies used for the simplicity of the system, ease of maintenance, as well as low cost [40].

When comparing the performance of the heat dissipation sink due to the difference in position on both the numerical and experimental levels, the position away from the source of the heat dissipation sink is the optimum position where the performance improves by 30% [41,42]. A comparison made by Ali et al. of two different pin-fin tank configurations (square and round) with two different phase-change materials [41]. Pins with fins under different cross-sections (circular, oval) with a mixed forced load has been studied by Deshmukh and Warkhedka [42]. An increase in the fin spacing leads to an increase in the spacer portion of the fin beam and, consequently, a decrease in thermal performance.

Many studies have been conducted to increase the efficiency of the heat sink, such as developing numerical and experimental models to reach the effect of adding an overlapping design of dimples and perforated dimples for multi-hole fins on heat transfer [43]. Numerical investigation on the effect of convective heat transfer and pressure drop in a heat sink through the effects of porous fins and a uniform external

magnetic field [44]. Obtaining heat sink for smooth surface and heat dissipation for finned mill with electrostatic spray cooling properties [45]. Fluid flow and heat transfer properties of open micro-channel heat sinks with square pin fins were investigated by a numerical study conducted by Prabhakar and Prajapati [46]. The numerical results of an investigation conducted on the effect of the fin length of a small channel containing an open space between the upper wall of the heat dissipation basin and the upper surface of the fin showed that the rate of heat transfer enhanced when the fin length increased to a value of 1.5 mm and decreased after that value. Finned sink for heat dissipation with copper metal flat bottom studied by Ong et al. [47]. The energy inputs were placed under forced and free heating, indicating that lower temperatures were achieved when the air was cooled by convection, and a higher heat loss coefficient was compared to natural convection. A heat sink with fins made of aluminum in the shape of a honeycomb under variables such as fin height, was analyzed numerically to verify the hydrothermal performance. The experimental results showed that when increasing fin height and Re and decreasing fin pitch ratio, thermal resistance value decreases [48].

Using the levenbery_marquardt method, the design problem of the pin fin array was studied to determine the best shape and perforation diameters for the perforated fin array unit based on the temperature difference between the ambient temperature and the average base plate temperature. The results showed that the perforation, the shorter height of the fin pin and the larger diameter gives the best heat dissipation performance [49]. A numerical investigation by Soleymani et al. has been conducted for determining heat transfer in a hybrid nanofin suggested a heat sink consisting of 143 finning pins in the hotspot region and 20 microchannels in the background region. The numerical results showed that the rate of heat transfer increases with the increase in the amplitude of the wall wave [50]. Whereas Wang et al. proposed a double-layer heat dissipation sink of corrugated porous ribs with a small channel. The small channel heat dissipation sink showed higher pumping force, and with the increase in the porous permeability or the decrease in the sq factor of the casting, the thermal resistance decreases [51]. Attar et al. presented a cost-effective and environmentally viable chemical method for constructing a rough structure on traditional aluminum basins, in order to increase the cooling potential in them. The simple method used in this study

sheds light on the possibility of using a heat sink with a specific size for thermal management of a higher heat flow system or reducing the size of aluminum heat sinks [52]. The properties of friction loss and heat transfer of multiple holes were studied by Tariq et al. in the heat of plate fins. Hence, the dissipation basin achieves an increase in the heat transfer coefficient over the flat fins that do not contain holes [53].

After literature review, it has been found that there is no adequate research showing the effect of changing different heat sink with pin fin parameters, so this research is a stimulating new horizon to literature. Where this research aims to study the thermal and hydraulic performance characteristics of the hexagonal pin fins.

Aim of the study: In this study, fluid flow and heat transfer characteristics of heat sink with pin fins have been analyzed numerically. The effects of variations of pitch ratio and diagonal length on the convective heat transfer have been determined. At the same time, the effect of variation of twisting ratios of the pin fins on convective heat transfer has also been analyzed in detail. As a result, the best and most practical design of a heat sink has been determined.

PART 3

METHODOLOGY

3.1. PHYSICAL MODEL

In the concept of this study, fluid flow and heat transfer characteristics in heat sink with pin fins has been determined numerically. Different pitch ratios, diagonal lengths, and twisting ratios of pin fins have been analyzed in detail. Numerical analyses have been performed under turbulent flow condition ($2658 \leq Re \leq 7138$). The turbulent flow condition was implemented in the transient region. The heat sink has been located in square cross-sectioned duct whose cross-sectional dimensions are 120 mm x 120 mm and a length of 500 mm. Detail view of computational domain and dimensions is presented in Figure 3.1. In this figure, L_{ef} [mm] represents the diagonal length of pin fins. F_L [mm] and L_d [mm] are the length of the pin fins and square cross-sectioned duct, respectively. p [mm] is the distance between the fins in spanwise direction while e [mm] is the distance between fins in streamwise direction. W_d [mm] is the dimension of the edge of the square cross-sectioned duct. The heat sink was made with 25 pin fins on the square surface with dimensions of 100 mm x 100 mm and fixed in the middle of the square cross-sectioned duct. Distance between fins has been taken constant as e=20 mm in the streamwise direction, while it has been changed in the spanwise direction with three different values as p=15 mm, 20 mm, and 22 mm (p/e=0.75, 1.0 and 1.1), respectively. Four different fin lengths have also been used in the numerical calculations (L_{ef}=3 mm, 4 mm, 5 mm and 6 mm). Besides, three different twisting ratios (TR=50, 100, 200) of pin fins have been analyzed.

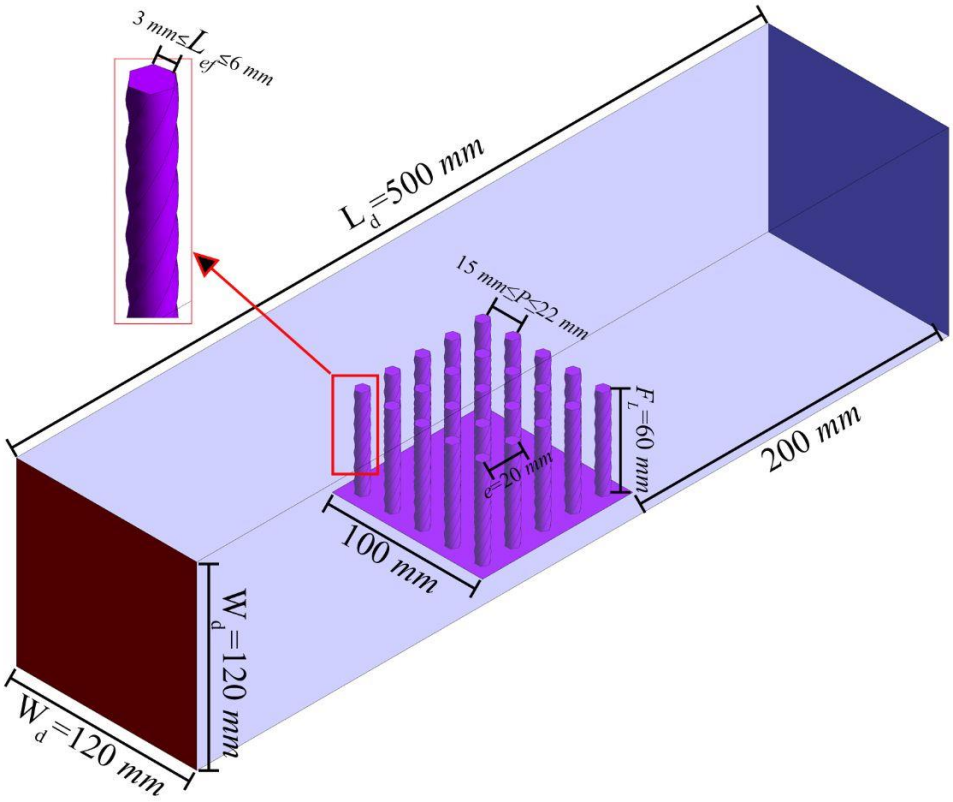

Figure 3.1. 3D view of computational domain with dimensions.

Twelve cases for each twisting ratio have been studied numerically in this study. Total 240 numerical calculations have been performed. The schematic views of each analyzed case are presented in Figure 3.2. Analyses have been conducted for three different distances between the pin fins ($0.75 \leq p/e \leq 1.1$), four different pin fin diagonal lengths ($3 \text{ mm} \leq L_{ef} \leq 6 \text{ mm}$) and three different twisting ratios of pin fins ($50 \leq TR \leq 200$).

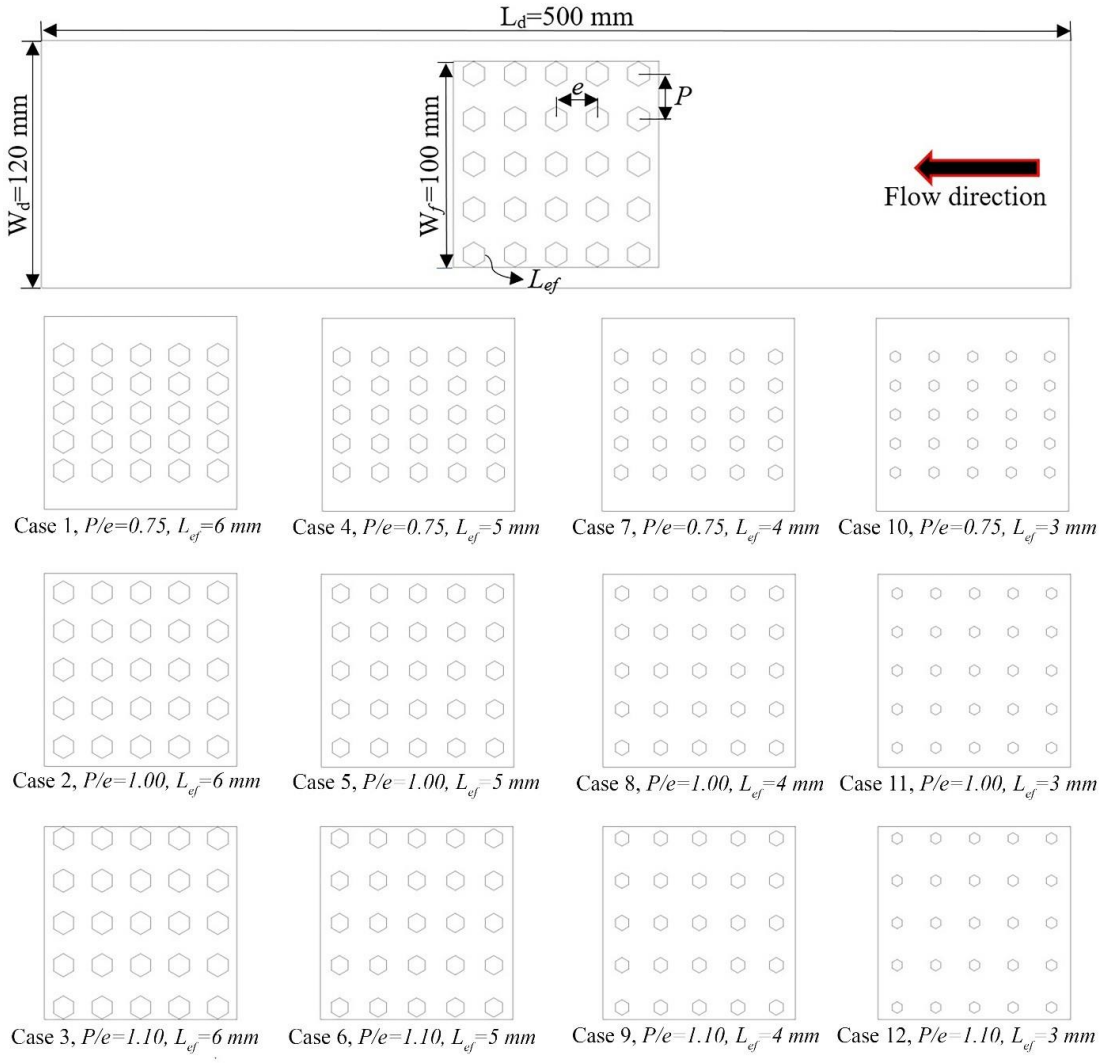

Figure 3.2. Schematic views of each case.

3.2. GOVERNING EQUATIONS

Conservation of Mass, Conservation of Momentum and Conservation of Energy equations have been solved numerically in this study. Since the problem has been analyzed under turbulent flow condition, Turbulence Equation has also been used. *SST k-ω* with low-*Re* correction model has been utilized for all analyses. Enhanced Wall Treatment model has been applied as the wall treatment model. The Governing Equations used in the calculations are presented in this section.

Conservation of Mass:

$$\frac{\partial p}{\partial t} + \frac{\partial (p u_i)}{dx} = 0 \qquad (3.1)$$

Conservation of Momentum:

$$\frac{\partial(pu_i)}{dt} + \frac{\partial(pu_i u_j)}{dx_j} = -\frac{\partial p}{\partial x_i} + \frac{\partial}{\partial x_j}\left[\mu\left(\frac{\partial u_i}{\partial u_j} + \frac{\partial u_j}{\partial x_i} - \frac{2}{3}\delta_y \frac{\partial u_i}{\partial x_j}\right)\right] + i\frac{\partial}{\partial x_j}(-pu`_i u`_j) \qquad (3.2)$$

Where u_i and u_j are the time-averaged velocity for i and j directions and $-pu`_i u`_j$ are presenting the Reynolds stresses.

Conservation of Energy:

$$\frac{\partial}{\partial t}(\rho E) + \frac{\partial}{\partial x_i}\lfloor u_i(\rho E + pr)\rfloor = \frac{\partial}{\partial t}\left[\left(k + \frac{cu_i}{pr_t}\right)\right]\frac{\partial T}{\partial x_j} + \mu_i(\tau_{ij})_{eff} \qquad (3.3)$$

Where ρ is density, k is turbulent kinetic energy, $(\tau_{ij})_{eff}$ is the deviatoric stress tensor.

Turbulence Equation:

$$\frac{\partial(pk)}{dt} + \frac{\partial(pku_i)}{dx_i} = \frac{\partial}{dx_j}\left[\Gamma_k \frac{\partial k}{dx_j}\right] + G_k - y_k + S_k \qquad (3.4)$$

Where p is time-averaged pressure and G_k is production of turbulent kinetic energy.

$$\frac{\partial(p\omega)}{dt} + \frac{\partial(p\omega u_i)}{dx_i} = \frac{\partial}{dx_j}\left[\Gamma_\omega \frac{\partial \omega}{dx_j}\right] + G_\omega - y_\omega + S_\omega \qquad (3.5)$$

The production of ω is given as G_ω, Γ_ω and Γ_k are undulating dilatation of the *k* and *ω*, respectively. y_k and y_ω present the dilatation of *k* and *ω* due to turbulence and S_k and S_ω are user-defined resource terms.

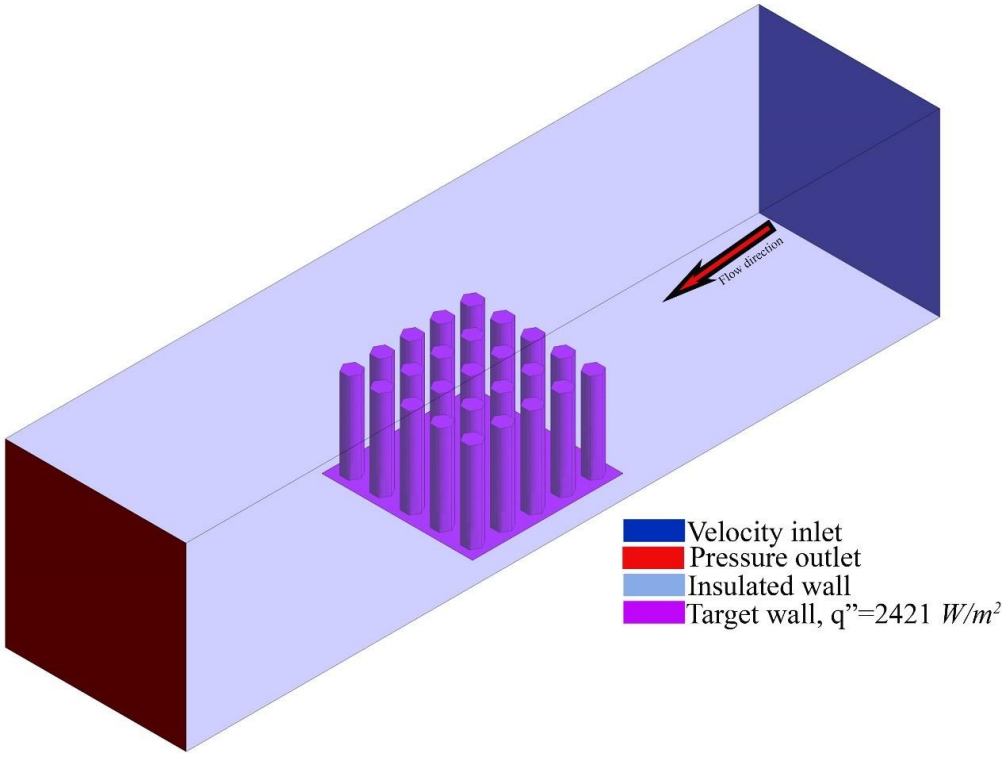

Figure 3.3. Explanation of computational domain and the boundary conditions.

Solving of the Governing Equations, boundary condition has been used. In this regard, uniform velocity and temperature boundary conditions have been applied at the inlet section of the square duct. Constant heat flux was applied at the bottom surface of the heat sink with $q^{"}$=2421.88 W/m^2. The other surfaces of the square duct have been kept adiabatic. No-slip boundary condition has also been applied at the surfaces of the duct and heat sink. At the outlet section of the square duct, pressure outlet boundary condition has been applied. The boundary conditions can be seen clearly in Figure 3.3.

3.3. SOLUTION PROCEDURE

ANSYS Fluent2020R2 commercial code was used for calculations. SIMPLE Method has been used for solving of Pressure-Velocity Coupling. Least Square Cell Based Method has been implemented for spatial discretization. For discretization of the Pressure, Momentum, Turbulent Kinetic Energy, Specific Dissipation Rate and Energy equations the second-order upwind scheme has been used for numerical analyses. The all-residual values have been reached 10^{-6} as a converging criterion. In

numerical analyses for Under Relaxation Factors for the properties and equations have been taken as; 0.3, 1.0, 1.0, 0.7, 0.8, 0.8, 1.0, 0.9 for Pressure, Density, Body Forces, Momentum, Turbulent Kinetic Energy, Specific Dissipation Rate, Turbulent Viscosity and Energy, respectively. Air is used as the working fluid of the study. Thermophysical properties of the air is given in Table 3.1.

Table 3.1. Thermophisical properties of air.

Thermal Conductivity $[W/mK]$	**Dynamic Viscosity** $[Pa.s]$	**Specific Heat** $[J/kgK]$	**Density** $[kg/m^3]$
0.02566	$1.858e^{-05}$	1007	1.176

The Reynolds number is calculated as follows:

$$Re = \frac{\rho V D_h}{\mu} \tag{3.6}$$

Where V [m/s], ρ [kg/m^3], and μ [kg/ms] are the average velocity, density and dynamic viscosity of air, respectively. D_h [m] is the hydraulic diameter of the square duct.

The hydraulic diameter is determined as flows:

$$\text{Dh}=\frac{4A_c}{p} = \frac{4a^2}{4a} = a \tag{3.7}$$

The convection heat transfer coefficient can be calculated as:

$$h = \frac{q''}{(T_w - T_b)} \tag{3.8}$$

where T_w [K] is the average surface temperature of heat sink, q'' [W/m^2] is the heat flux, and T_b [K] is the average temperature of inlet and outlet temperatures.

Using convection heat transfer coefficient average Nusselt number can be calculated by:

$$Nu = \frac{hD_h}{k} \tag{3.9}$$

where, k [W/m.K] is the thermal conductivity of the air.

Darcy friction factor can also be calculated as:

$$f = \frac{2D_h \times \Delta P}{L_d \times \rho \times V^2} \tag{3.10}$$

where, ΔP [Pa] is the pressure loss in the duct.

Thermal resistance of the pin fins can be calculated:

$$R = \frac{T_{avg.,HS} - T_{in}}{q^{"}} \tag{3.11}$$

where, $T_{avg.,HS}$ [K] is the average wall temperature of the heat sink, and T_{in} [K] is the inlet temperature.

Also, the Performance Evaluation Criteria (*PEC*) is important parameter to evaluate the overall performance of a heat sink and it can be calculated by:

$$PEC = \frac{(Nu^*/Nu^0)}{(f^*/f^0)} \tag{3.12}$$

Where, Nu^* is Nusselt number for certain case, Nu^0 is Nusselt number for the case of *TR*=0, f^* is friction factor for certain case, and f^0 is the friction factor of *TR*=0 case.

Turbulent intensity has also been calculated by:

$$I = 0.16Re^{\left(-\frac{1}{8}\right)} \tag{3.13}$$

3.4. MESH INDEPENDENCE STUDY

In order to ensure that the results of the analysis change with the change of the mesh structure, the mesh independence must be studied. Therefore, this study is considered one of the important things that must be done to determine the best mesh structure. In this regard, eight different mesh structured have been carried out in the ANSYS Mesher. The all-mesh studies have been performed for Case 2 at *Re*=7138 and *q"* =2421 W/m^2. as shown in Figure 3.4. It is seen in the figure that there is no significant change in the average Nusselt number and average Darcy friction factor after the sixth study of the simulations. Based on this condition, the sixth mesh structure with an element number of 1194130 was chosen as an optimum mesh structure for this study. And this mesh structure has been used all the simulations.

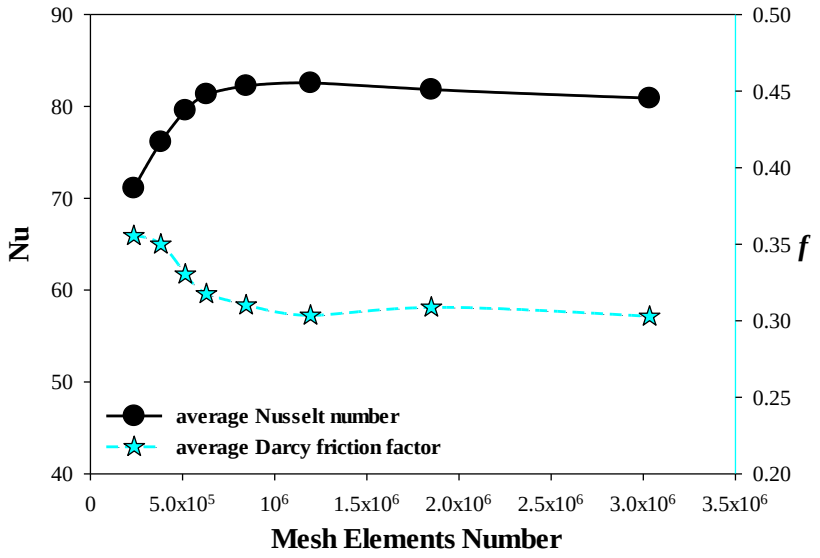

Figure 3.4. Mesh independence study at *Re* =7138.

The denser mesh optimization must be applied on the surfaces where the fluctuations are high (Figure 3.5). In this study, the denser mesh has been applied for inlet, outlet of the duct and onto the heat sink placed at the middle of the duct. Also, the aspect ratio, orthogonal quality, skewness values, which define the quality of the mesh structure, have been monitored for each analysis to examine calculation quality. It is noted that there is another criterion determining analysis quality norm, which is namely normalized distance from the wall (y^+). When the *SST k-ω* with low-*Re*

correction model is used, the y^+ value should be lower than *1.0* to obtain feasible calculation near the walls. For this purpose, the y^+ value has kept almost 0.4 for each case.

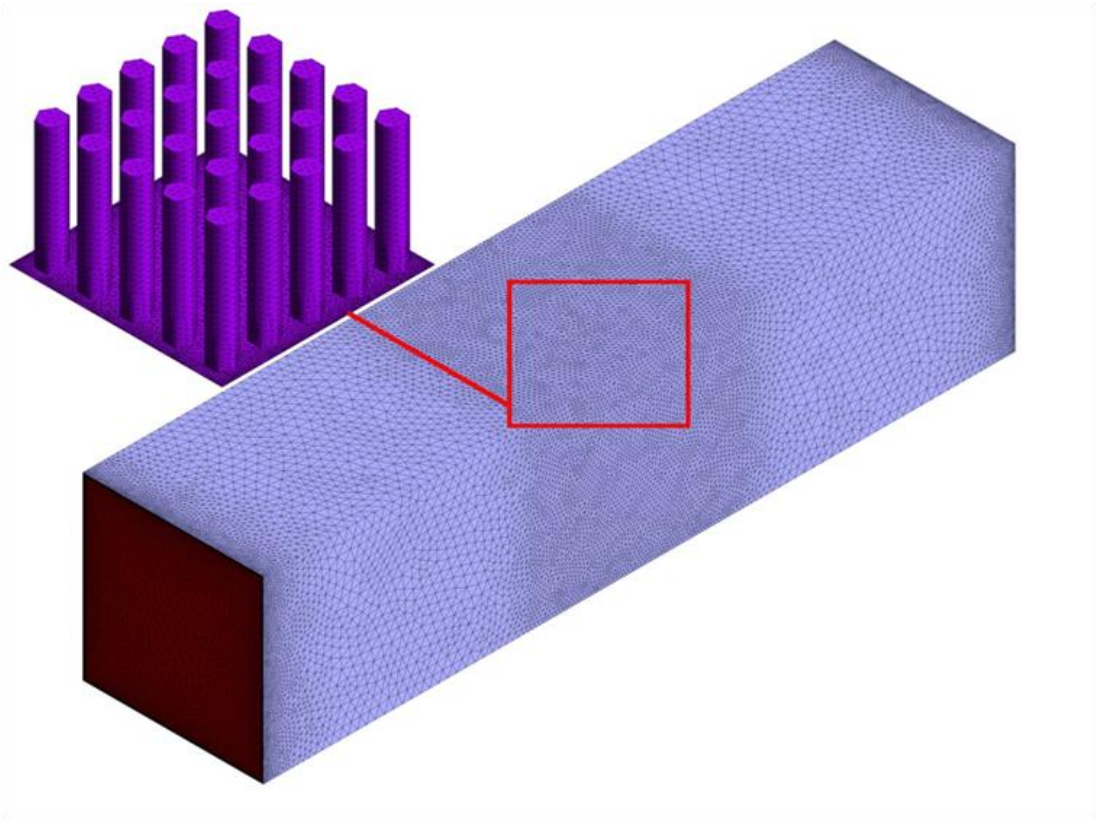

Figure 3.5. Mesh structure of computational domain

3.5. SELECTION OF TURBULENCE MODEL AND VALIDATION OF THE STUDY

In order to conduct a study under turbulent flow condition, suitable turbulence model must be defined. In this regard, four different turbulence models (*SST k-ω, Transition SST, RNG k-ε and Realizable k-ε*) have been tested and compared with the experimental data of El-Said's experimental investigation [1]. The numerical results with data obtained from literature are given in Figure 3.6. It is obtained from the figure that *SST k-ω* turbulence model is the most suitable model since it gives the lowest deviation rate compared to other models, reaching about 4.0% for average Nusselt number compared to the experimental data of El-Said et al. [1]. *Transition SST, RNG k-ε and Realizable k-ε* turbulence models gives exaggerated deviation from the

experimental data with 6.0%, 9.0% and 10.72%, respectively. As a result, it has been obtained that the results of the numerical study are in harmony with the literature and the computational domain is reliable.

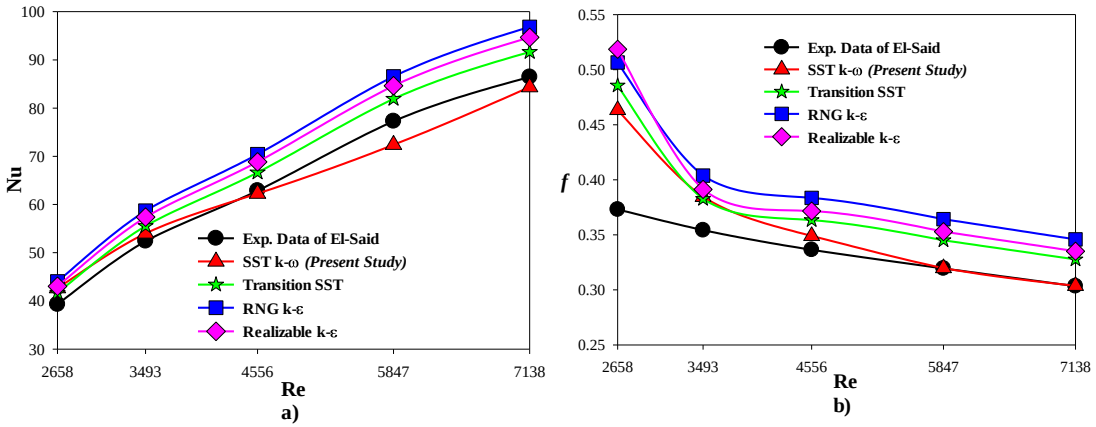

Figure 3.6. Variation of a) Average Nusselt number, b) Variation of average Darcy friction factor, with Reynolds number for different turbulence models [1].

PART 4

RESULTS AND DISCUSSION

In this numerical study, the effects of variations of pitch ratio and diagonal length of pin fins located in heat sink on the convective heat transfer have been determined. The effect of variation of twisting ratios of the pin fins on convective heat transfer has also been analyzed in detail. In this regard, 240 numerical calculations have been carried out. Numerical findings are presented and discussed in this part for each case. Results are given as variations of average Nusselt number, average Darcy friction factor, thermal resistance, and *PEC* with Reynolds number. Surface Nusselt number, temperature, and vorticity distributions are analyzed in detail. Velocity streamlines have also been drawn for different cases.

4.1. STRAIGHT (UNTWISTED) PIN FIN CONDITION (*TR*=0)

In this case, calculation results for straight (untwisted) pin fin condition (*TR*=0) are presented and discussed in detailed. Variations of average Nusselt number with Reynolds number are presented in Figure 4.1 for each case. It can be seen in this figure that average Nusselt number increases with increasing Reynolds number. The highest heat transfer rate is reached in Case 12, whereas lowest one is in Case 1 for all Reynolds numbers. It can also be obtained that decreasing diagonal length and increasing pitch ratio increase the heat transfer rate on the heat sink. The maximum average Nusselt number is determined as 101.834 for *Re*=7138.

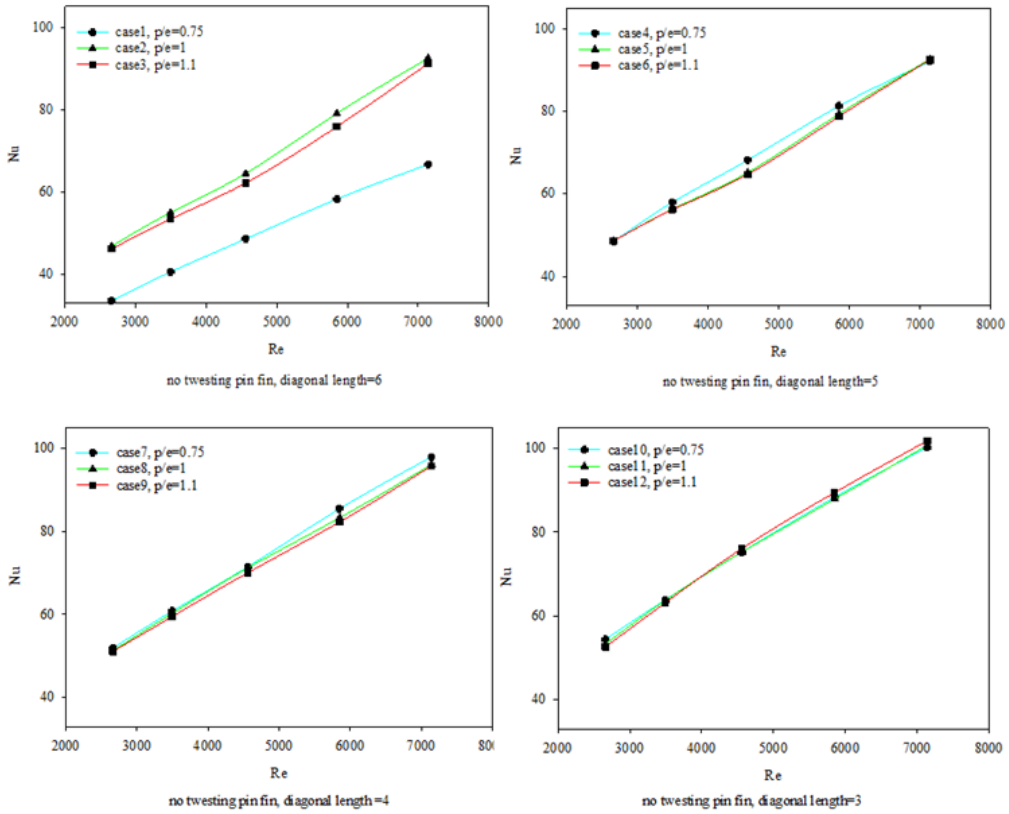

Figure 4.1. Variation of average Nusselt number with Reynolds number in different cases for *TR*=0.

The surface Nusselt number distribution on the heat sink at *Re* =7138 for different cases can be seen in Figure 4.2. It is determined that reducing the diagonal length of the pin fin provides a more stable flow over the heat sink and it increases the surface Nusselt number. It can also be seen that the surface Nusselt number decreases in the streamwise direction.

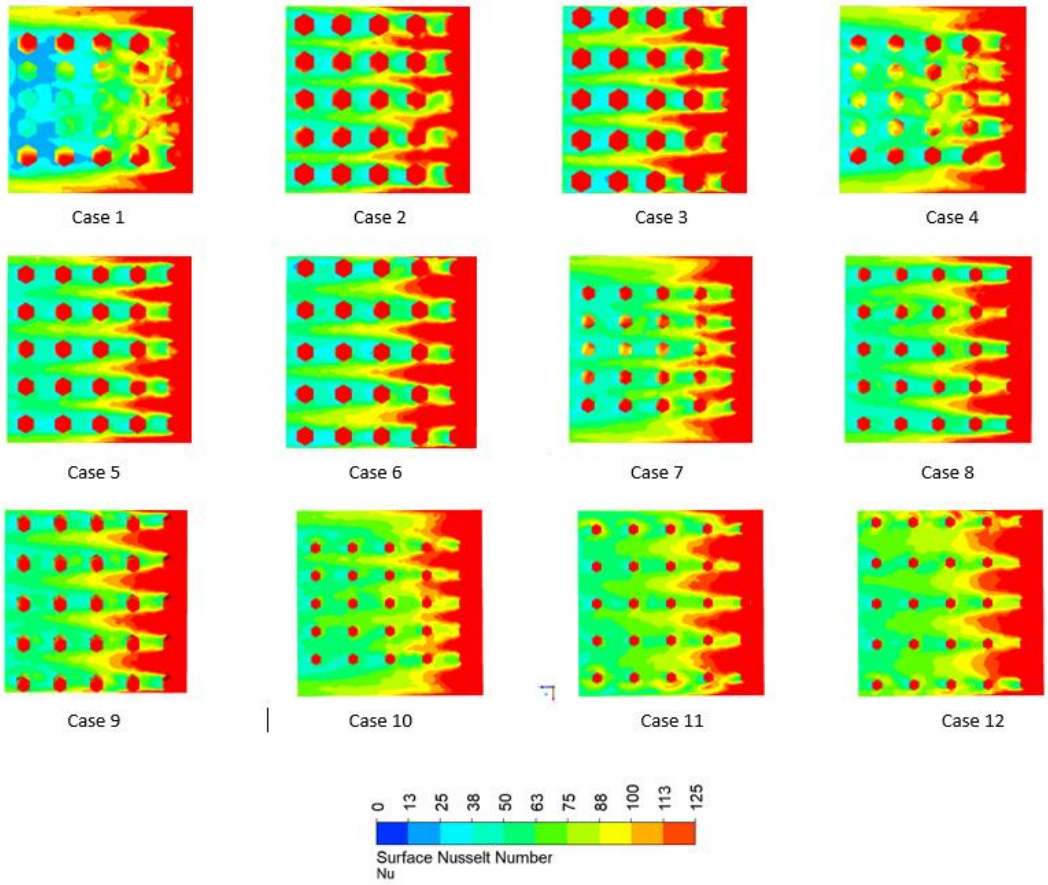

Figure 4.2. Surface Nusselt number distribution over the heat sink for different cases and *TR*=0 at *Re*=7138.

Deciding the configuration is acceptable or not, it is important parameter to obtain the hydraulic performance of the novel heat sink design and it is also important in terms of research, innovation, and commercialization. To illustrate the hydraulic performance of the heat sink, variation of average Darcy friction factor with Reynolds number for different cases is presented in Figure 4.3. It can be revealed from the figure that average Darcy friction factor decreases with Reynolds number. The maximum average Darcy friction factor has been obtained at Case 1, whereas minimum one is at Case 12. Since Case 12 gives the highest heat transfer rate and lowest pressure loss, the best case is the Case 12 for the untwisted pin fin condition (*TR*=0).

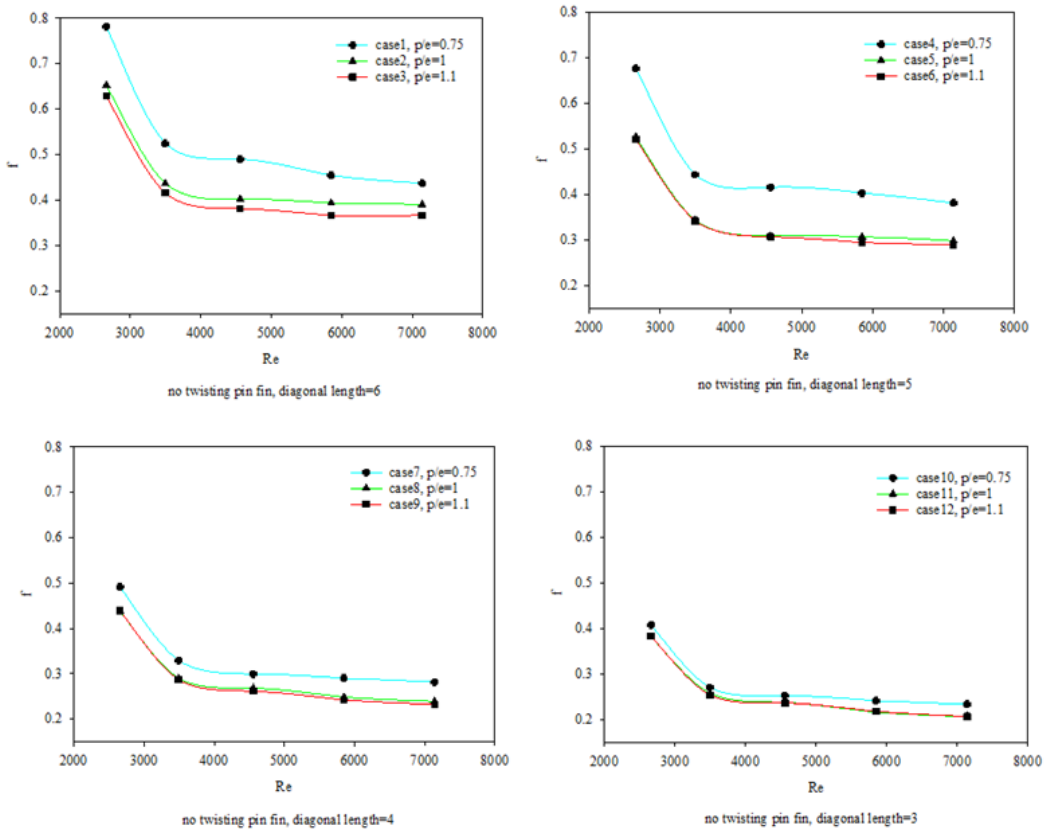

Figure 4.3. Average Darcy friction factor with Reynolds number in different diagonal lengths for *TR*=0.

Surface temperature distribution over the heat sink is given in Figure 4.4 at *Re*=7138. Surface temperature magnitude on the heat sink is maximum in Case 1 and minimum in Case 12. It can also be said that the maximum effective cooling in heat sink is achieved in Case 12, whereas minimum is in Case1. Less cooling is obtained over the heat sink at the wider diagonal length. Increasing interaction of the heat sink and coolant fluid the narrower diagonal length leads to greater cooling over the heat sink for all cases. That is the reason for obtaining more convective heat transfer rate.

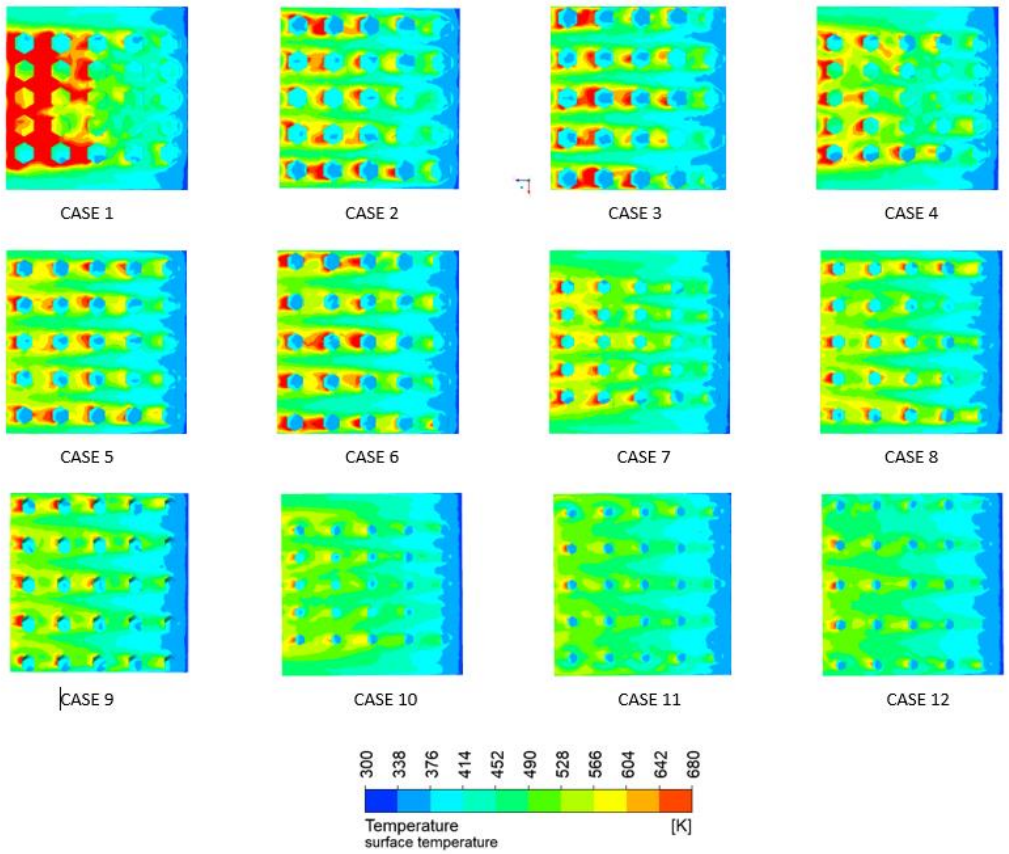

Figure 4.4. Surface temperature distribution over the heat sink in different cases at *Re*=7138 for *TR*=0.

Variation of average heat transfer of heat sink is given in Figure 4.5. The average heat sink temperature in Case 12 is lower compared to the other cases, in despite of the wider pitch ratio of the pin fins and the lower diagonal length. Faster flow between the pin fins and the heat sink surface and higher heat transfer rate and lower average surface temperature for all Reynolds numbers are obtained when using a small diagonal length with a high pitch ratio. Whereas, the maximum average temperature of the heat sink is reached at the lowest Reynolds number, the minimum average temperature of the heat sink is obtained at the highest Reynolds numbers.

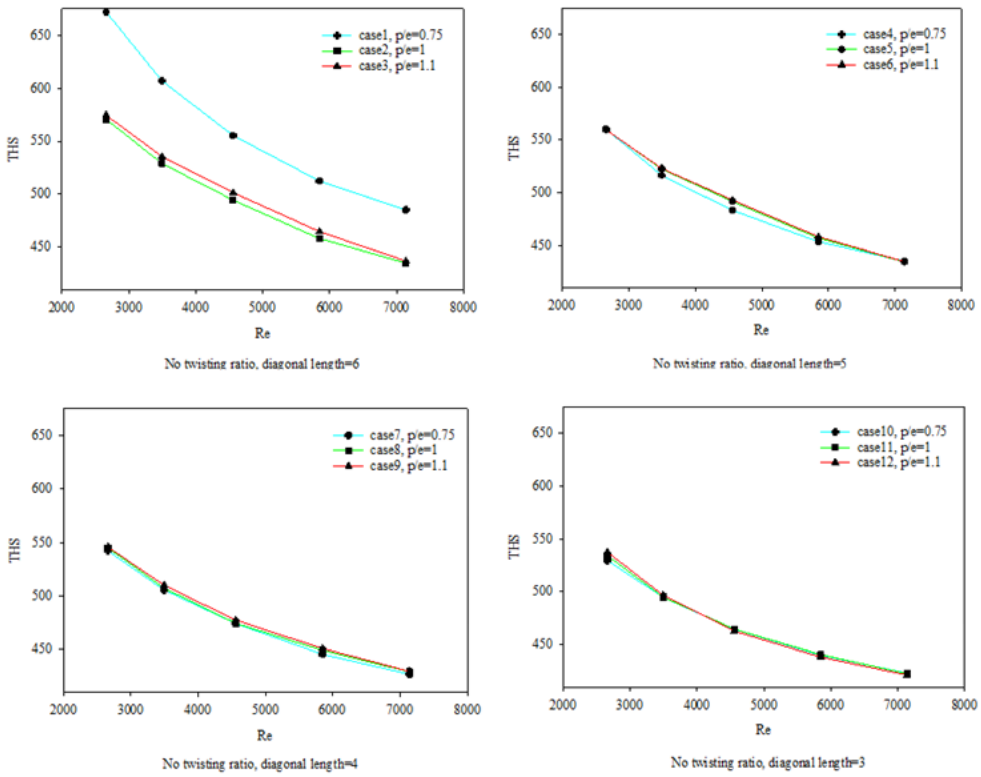

Figure 4.5. Variation of average temperature of heat sink in different cases for *TR*=0.

Thermal resistance is another important parameter of the heat sink applications. Variation of the thermal resistance with Reynolds number for different cases is given in Figure 4.6. The comparatively low average temperature of the heat sink gives the lower thermal resistance. So, lower thermal resistance is obtained in Case 12, and the higher one is in Case 1. Decreasing thermal resistance results in a positive effect on the performance of convective heat transfer.

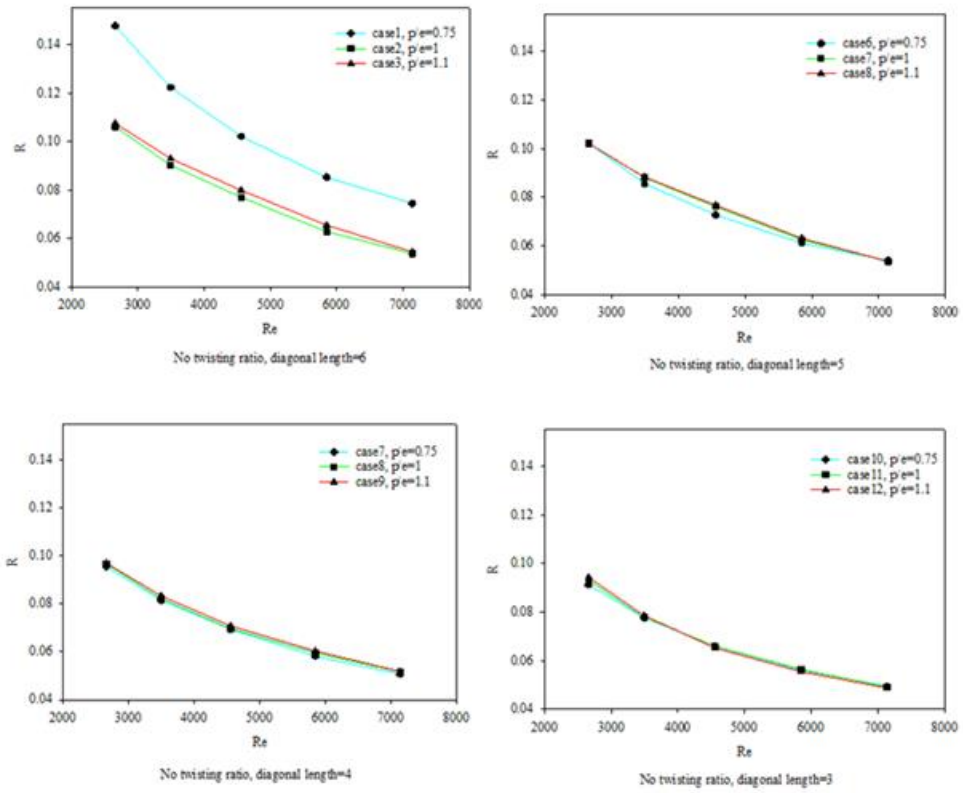

Figure 4.6. Variation of thermal resistance with Reynolds number in different cases for *TR*=0.

The features of the vorticity distribution on the heat sink are presented in Figure 4.7 for different cases at *Re*=7138. The plane surface has been generated 5 mm from the surface of heat sink for taking the contour graph. The vorticity distribution has been taken on this plane surface. Strong vortices occurred on the upper and lower surfaces in the horizontal direction, and in the vertical direction at the beginning of the heat sink and the first column of pin fins due to the increase in fluid velocity. Due to the uniform distribution of fluid flow between the pin fins, a decrease in vorticity occurs when the diagonal length of the pin fins is reduced, and the pitch ratio increases. With an increase in the pitch ratio on the lower surface of the heat sink, the vortices are taken higher, and when the diagonal length decreases on the tup-surface of the pin, the vortices occur less. Heat transfer rate is enhanced by reducing radial length and increasing pitch ratio, results in the occurrence of more uniformity and stronger rotation over the heat sink.

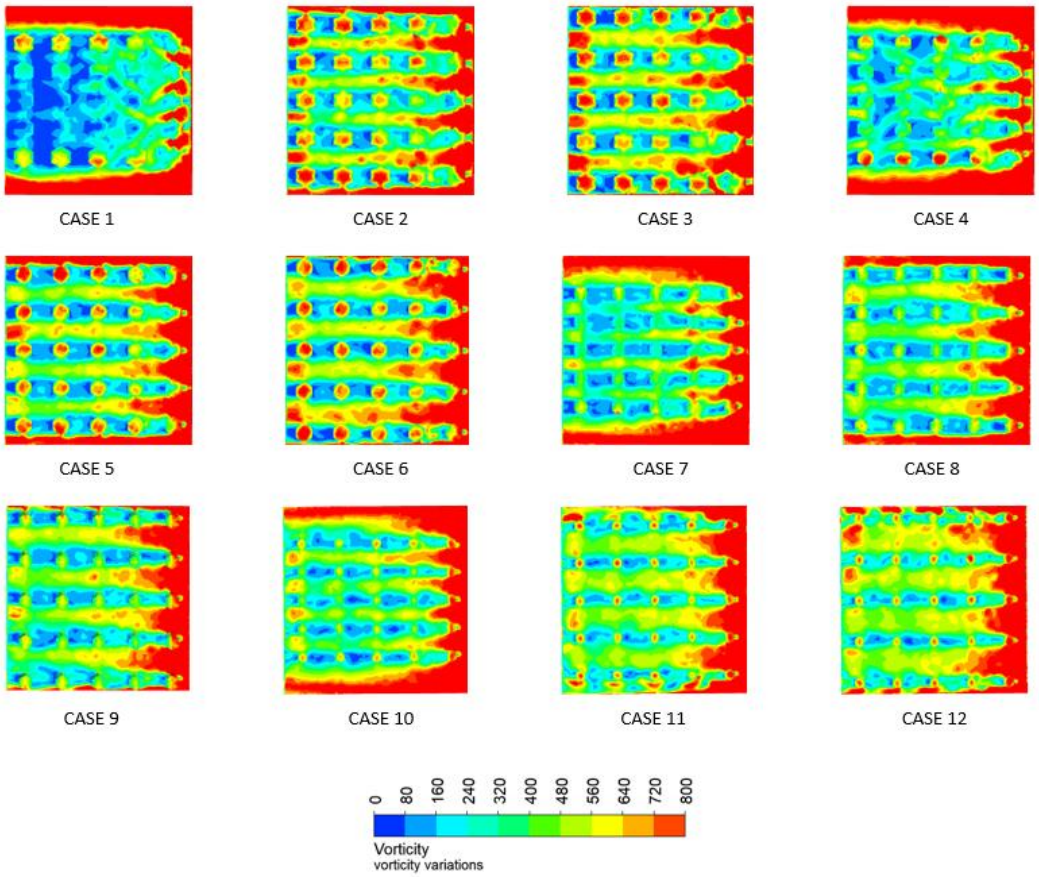

Figure 4.7. Vorticity distribution over the heat sink in different cases for *TR*=0.

Temperature streamlines on the generated plane surface at *Re*=7138 for different cases is given in Figure 4.8. As shown in Case 1 and Case 4, the velocity of the coolant is relatively high at the beginning of the heat sink, while it decreases with the movement of the fluid in the direction of the streamline due to the denser formation of the pin fins. More uniform streamline over the heat sink is achieved and so higher convective heat transfer rate with the decrease in diagonal length and increase in pitch ratio.

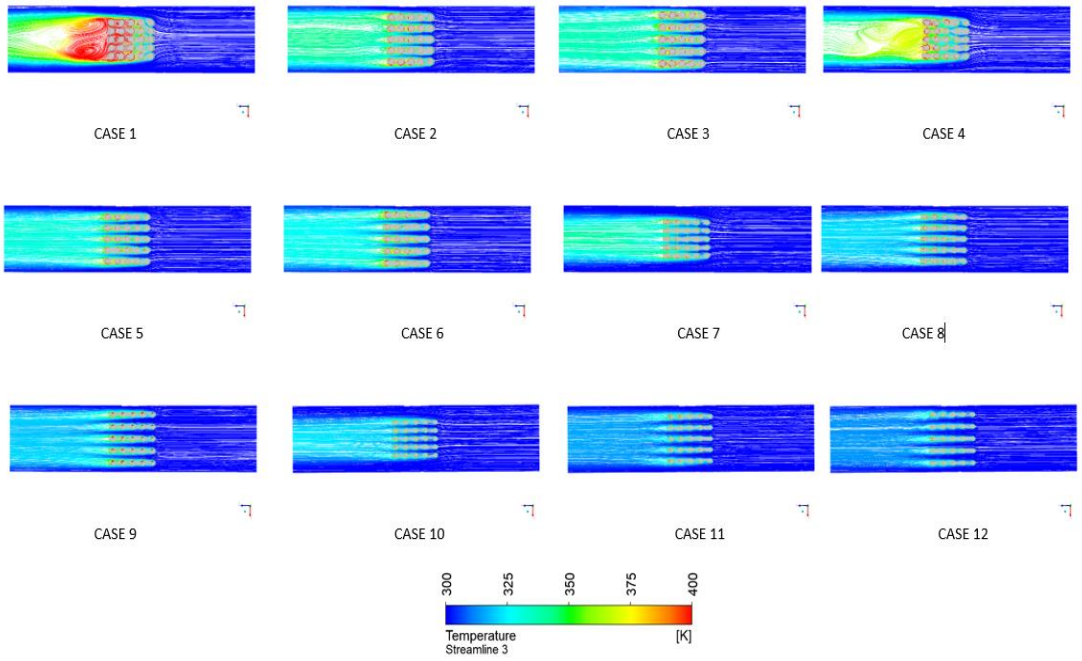

Figure 4.8. Temperature streamline distribution toward flow direction for different cases for *TR*=0.

4.2. TWISTED PIN FINS WITH *TR*=200

In this case, calculation results for pin fins with 200 twisting ratio condition (*TR*=200) are presented and discussed in detailed. And all the previous procedures have been repeated starting with Variations of average Nusselt number with Reynolds number which presented in Figure 4.9. for each case. It can be seen in this figure that average Nusselt number increases with increasing Reynolds number. The highest heat transfer rate is reached in Case 10, whereas lowest one is in Case 1 for all Reynolds numbers. It can also be obtained that decreasing diagonal length and increasing pitch ratio increase the heat transfer rate on the heat sink. The maximum average Nusselt number is determined as 100.419 for *Re*=7138

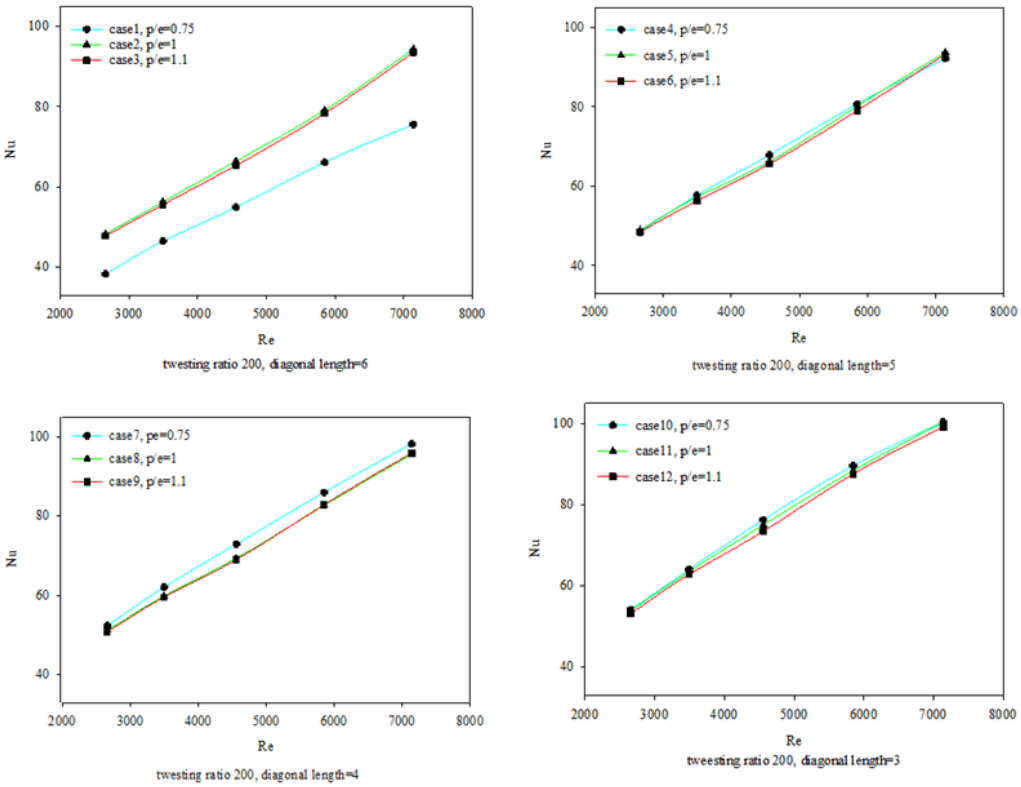

Figure 4.9. Average Nusselt number with Reynolds number in different cases for *TR*=200.

The surface Nusselt number distribution on the heat sink at *Re* =7138 for different cases can be seen in Figure 4.10. It is determined that reducing the diagonal length of the pin fin provides a more stable flow over the heat sink and it increases the surface Nusselt number. It can also be seen that the surface Nusselt number decreases in the streamwise direction.

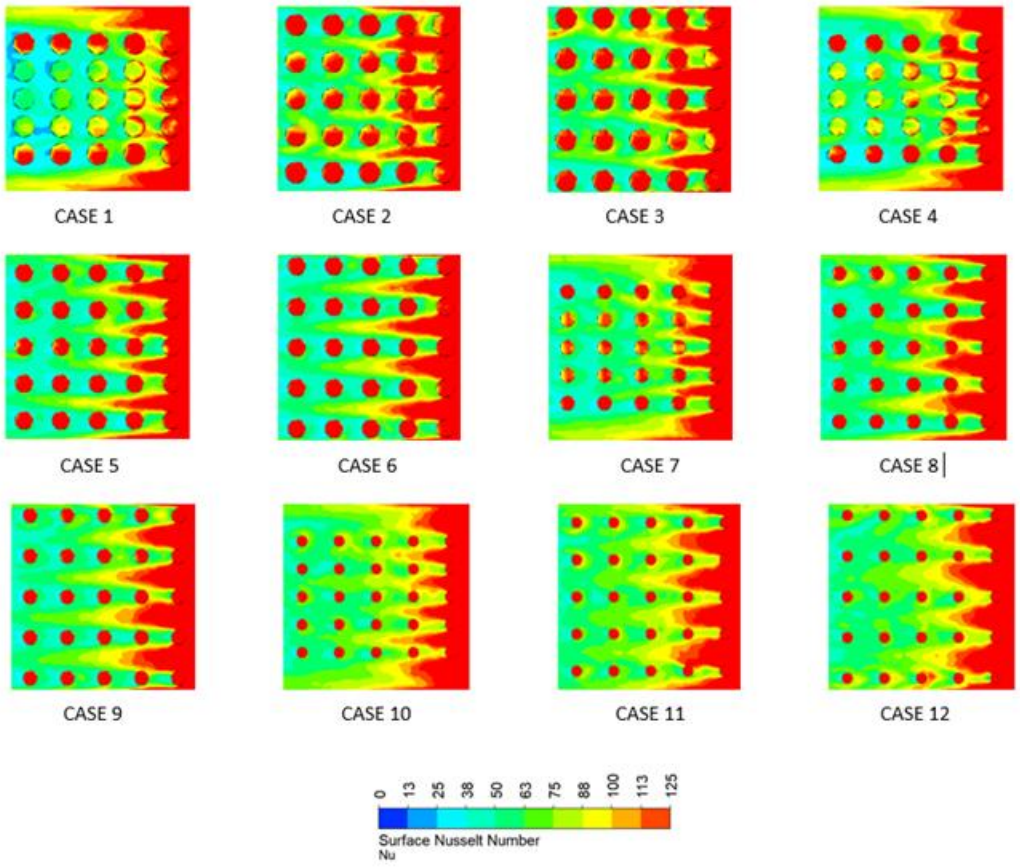

Figure 4.10. Surface Nusselt number distribution over the heat sink in different cases at *Re*=7138 for *TR*=200.

Deciding the configuration is acceptable or not, it is important parameter to obtain the hydraulic performance of the novel heat sink design and it is also important in terms of research, innovation, and commercialization. To illustrate the hydraulic performance of the heat sink, variation of average Darcy friction factor with Reynolds number for different cases is presented in Figure 4.11. It can be revealed from the figure that average Darcy friction factor decreases with Reynolds number. The maximum average Darcy friction factor has been obtained at Case 1, whereas minimum one is at Case 12. Since Case 12 gives the highest heat transfer rate and lowest pressure loss, the best case is the Case 12 for the pin fins with 200 twisting ratio (*TR*=200).

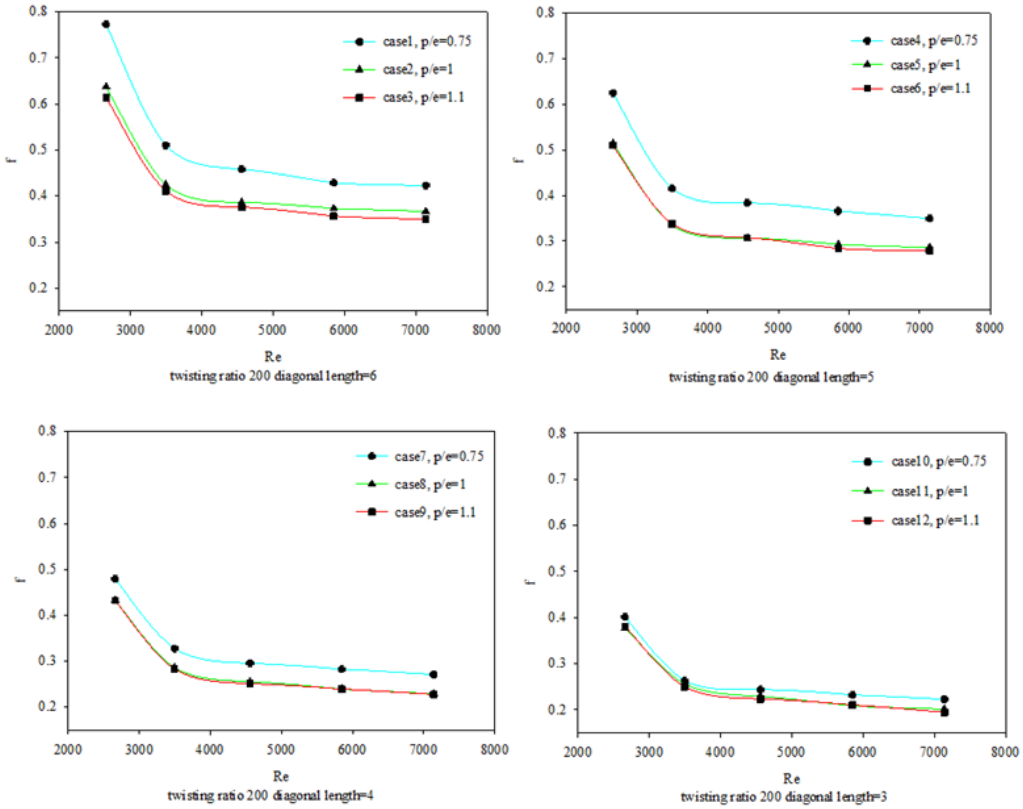

Figure 4.11. Average Darcy friction factor with Reynolds number in different diagonal lengths for *TR*=200.

Static temperature distribution over the heat sink is given in Figure 4.12 at *Re*=7138. Temperature magnitude on the heat sink is maximum in Case 1 and minimum in Case 12. It can also be said that the maximum effective cooling in heat sink is achieved in Case 12, whereas minimum is in Case1. Less cooling is obtained over the heat sink at the wider diagonal length, while due to the increased interaction of the heat sink and coolant fluid the narrower diagonal length leads to greater cooling over the heat sink for all cases. That is the reason for obtaining more convective heat transfer rate.

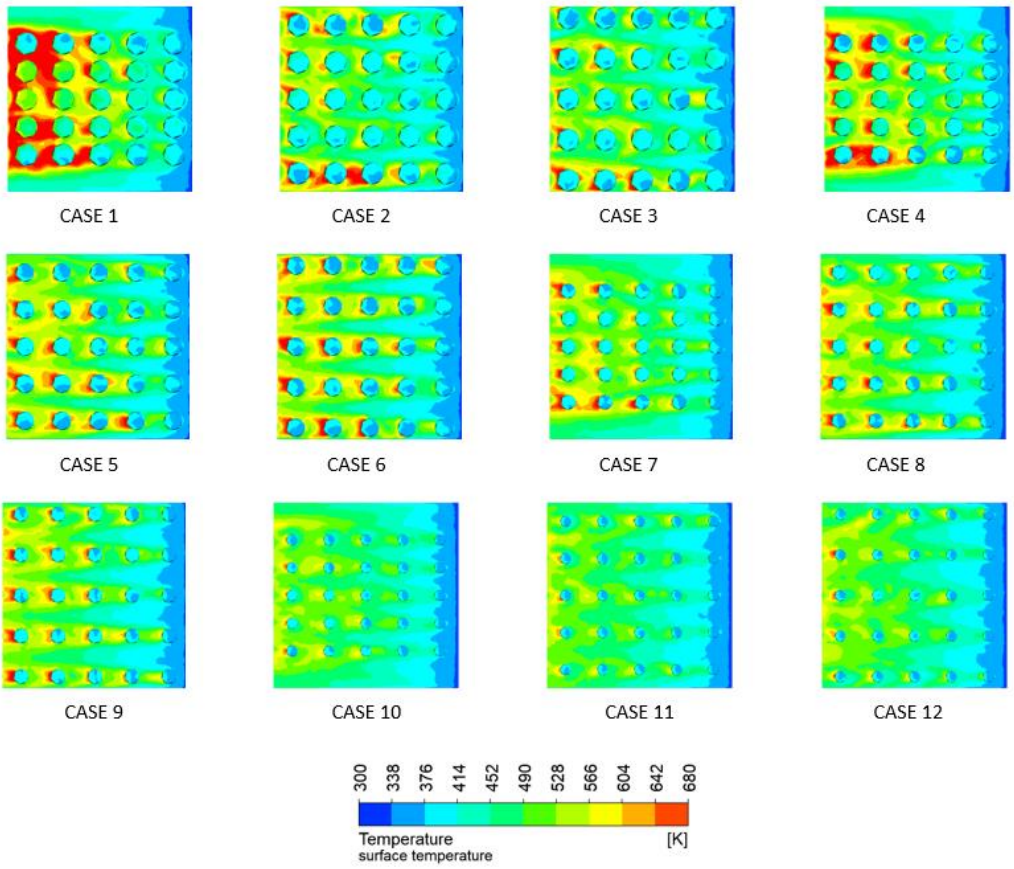

Figure 4.12. Static temperature distribution over the heat sink in different cases at *Re*=7138 with *TR*=200.

Variation of average temperature of heat sink is given in Figure 4.13. The average heat sink temperature in case No. 12 is lower compared to the other cases, in despite of the wider pitch ratio of the pin fins and the lower diagonal length. Faster flow between the pin fins and the heat sink surface and higher heat transfer rate and lower average surface temperature for all Reynolds numbers are obtained when using a small diagonal length with a high pitch ratio. Whereas, the maximum average temperature of the heat sink is reached at the lowest Reynolds number, the minimum average temperature of the heat sink is obtained at the highest Reynolds numbers.

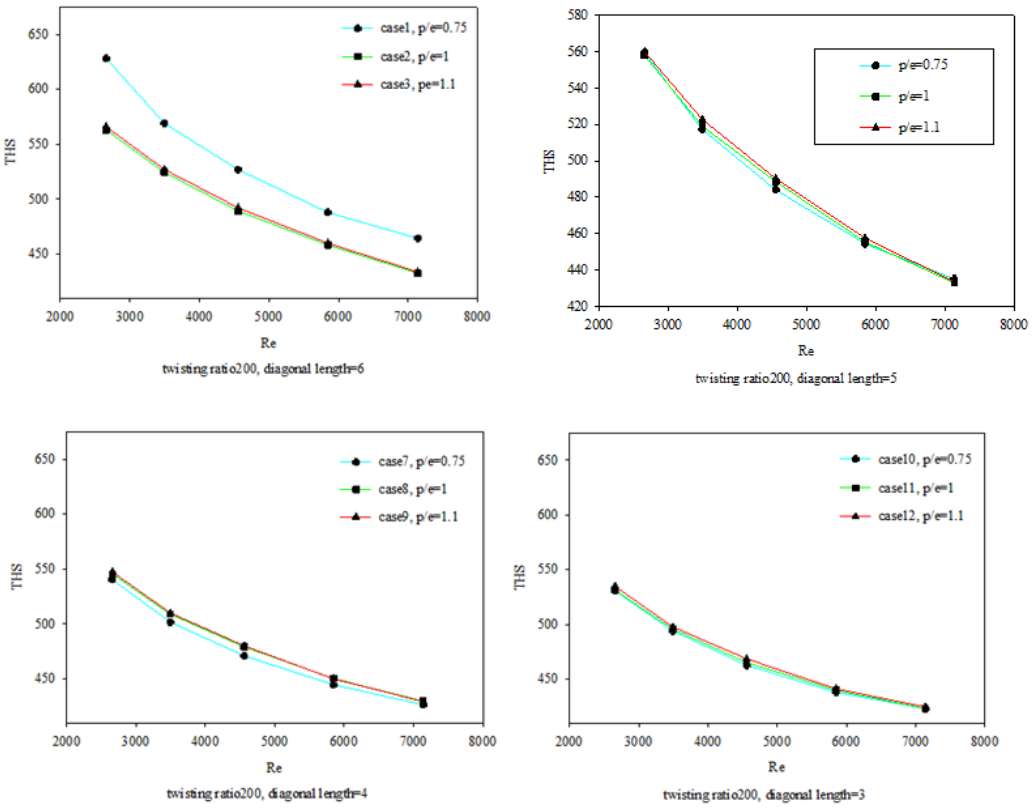

Figure 4.13. Variations of average temperature of heat sink for all cases for *TR*=200.

Thermal resistance is another important parameter of the heat sink applications. Variation of the thermal resistance with Reynolds number for different cases is given in Figure 4.14. The comparatively low average temperature of the heat sink gives the lower thermal resistance. So, lower thermal resistance is obtained in Case 12, and the higher one is in Case 1. Decreasing thermal resistance results in a positive effect on the performance of convective heat transfer.

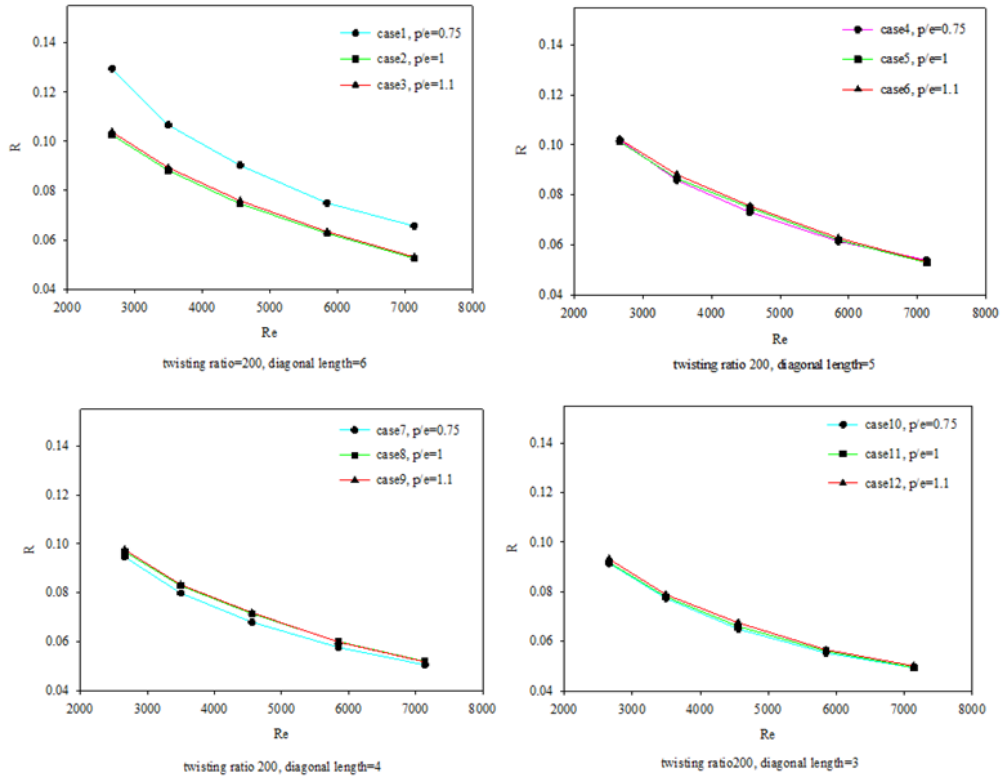

Figure 4.14. Thermal resistance with Reynolds number for all cases for *TR*=200.

The features of the vorticity distribution on the heat sink are presented in Figure 4.15 for different cases at *Re*=7138. The plane surface has been generated 5 mm from the surface of heat sink for taking the contour graph. The vorticity distribution has been taken on this plane surface. Strong vortices occurred on the upper and lower surfaces in the horizontal direction, and in the vertical direction at the beginning of the heat sink and the first column of pin fins due to the increase in fluid velocity. Due to the uniform distribution of fluid flow between the pin fins, a decrease in vorticity occurs when the diagonal length of the pin fins is reduced, and the pitch ratio increases. With an increase in the pitch ratio on the lower surface of the heat sink, the vortices are taken higher, and when the diagonal length decreases on the top surface of the pin, the vortices occur less. Heat transfer rate is enhanced by reducing radial length and increasing pitch ratio, results in the occurrence of more uniformity and stronger rotation over the heat sink.

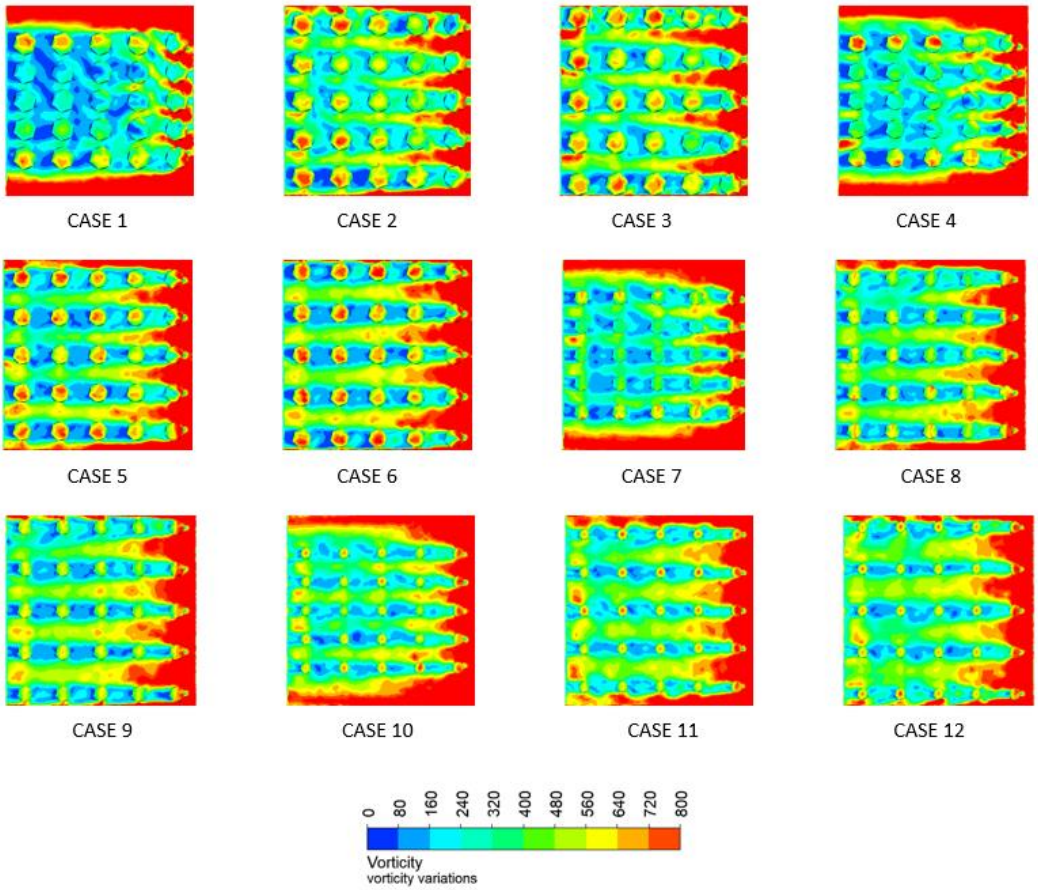

Figure 4.15. Vorticity variations over the heat sink in different cases at *Re*=7138 for *TR*=200.

Temperature streamlines on the generated plane surface at *Re*=7138 for different cases is given in Figure 4.16. As shown in Case 1 and Case 4, the velocity of the coolant is relatively high at the beginning of the heat sink, while it decreases with the movement of the fluid in the direction of the streamline due to the denser formation of the pin fins. More uniform streamline over the heat sink is achieved and so higher convective heat transfer rate with the decrease in diagonal length and increase in pitch ratio.

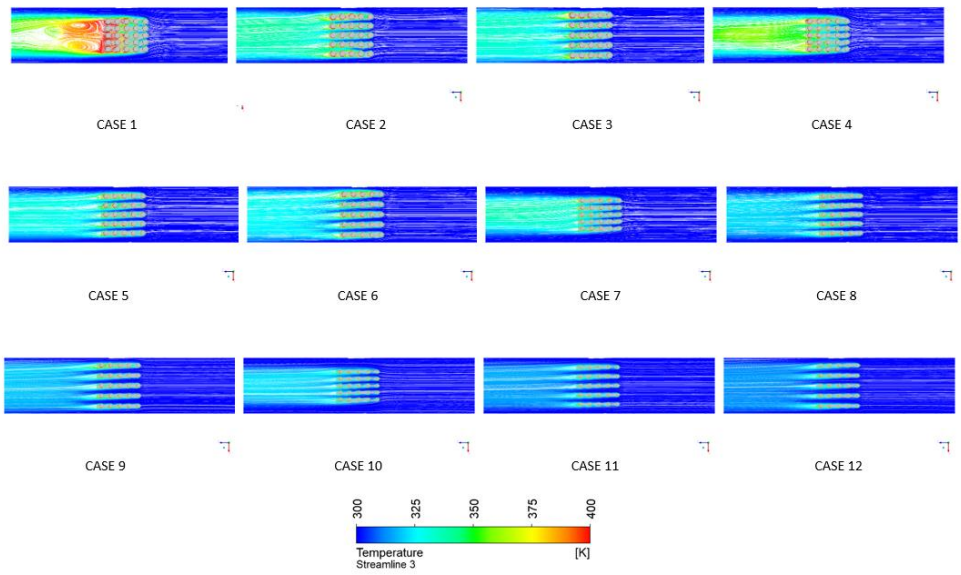

Figure 4.16. Temperature streamline toward streamwise direction for all cases at *Re*=7138 for *TR*=200.

Also, one of the important parameters is the *PEC* number which can be seen in Figure 4.17. For all the cases in different diagonal length noticing clearly that the *PEC* number decreases after Case 1 and stays almost stable for the rest of the cases. It is obtained that Case 1 is the most efficient case for the case of twisted pin fins with *TR*=200. It is also seen that twisting of the pin fin for other cases does not affect on the thermal performance since *PEC* numbers are almost unity.

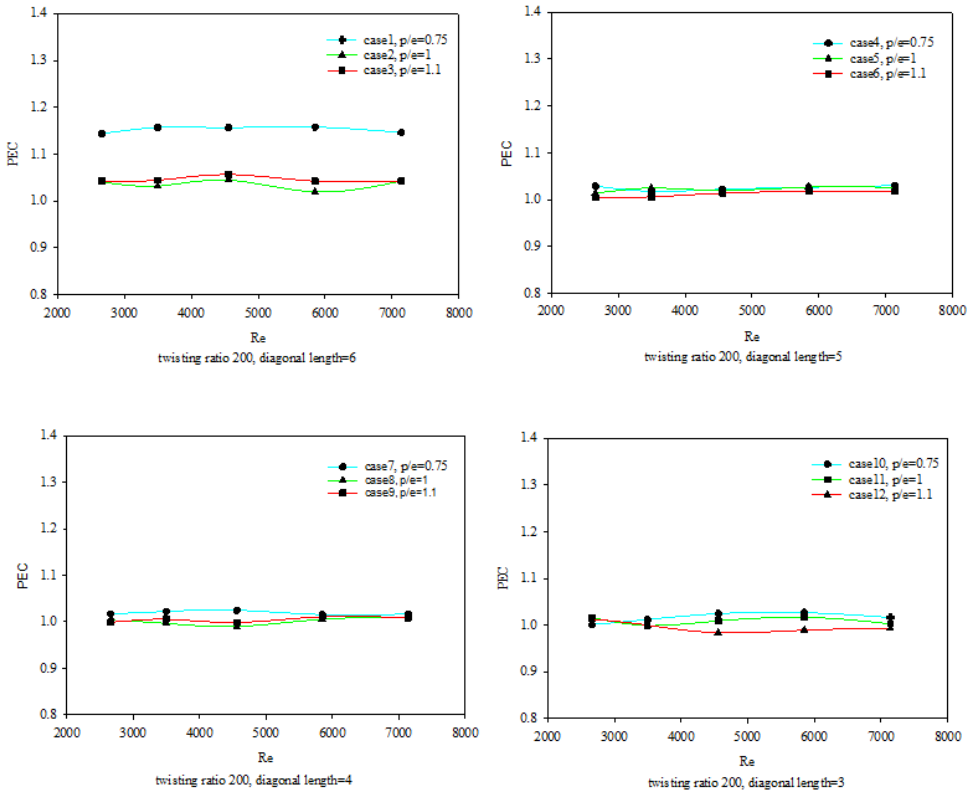

Figure 4.17. *PEC* number for all cases at different Reynolds numbers for *TR*=200.

4.3. TWISTED PIN FINS WITH *TR*=100

In this case, calculation results for pin fin with 100 twisting ratio conditions (*TR*=100) are presented and discussed in detailed. Variations of average Nusselt number with Reynolds number are presented in Figure 4.18 for each case. It can be seen in this figure that average Nusselt number increases with increasing Reynolds number. the highest heat transfer rate is reached in Case 10, whereas lowest one is in Case 1 for all Reynolds numbers. It can also be obtained that decreasing diagonal length and increasing pitch ratio increase the heat transfer rate on the heat sink. The maximum average Nusselt number is determined as 101.46 for *Re*=7138 is obtained by increasing pitch ratio and decreasing diagonal length.

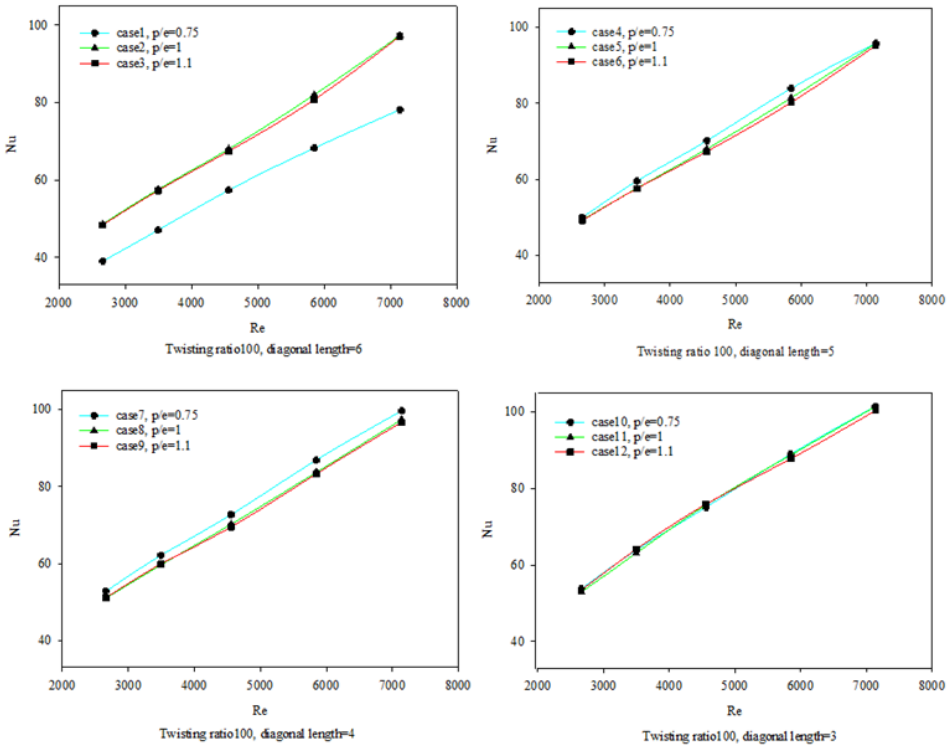

Figure 4.18. Average Nusselt number with Reynolds number in different cases for *TR*=100.

The surface Nusselt number distribution on the heat sinks at *Re* =7138 for different cases can be seen in Figure 4.19. It is determined that reducing the diagonal length of the pin fin provides a more stable flow over the heat sink and it increases the surface Nusselt number. It can also be seen that the surface Nusselt number decreases in the streamwise direction.

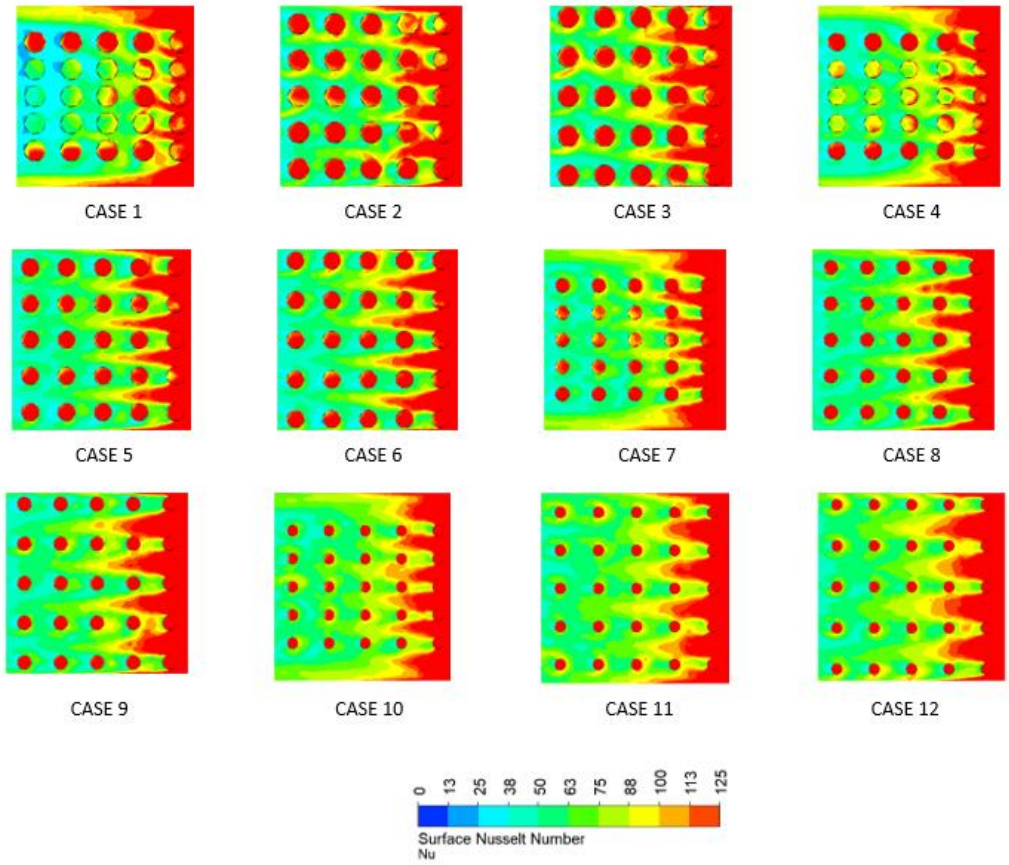

Figure 4.19. Surface Nusselt number distribution over the heat sink in different cases at *Re*=7138 for *TR*=100

Deciding the configuration is acceptable or not, it is important parameter to obtain the hydraulic performance of the novel heat sink design and it is also important in terms of research, innovation, and commercialization. To illustrate the hydraulic performance of the heat sink, variation of average Darcy friction factor with Reynolds number for different cases is presented in Figure 4.20. It can be revealed from the figure that average Darcy friction factor decreases with Reynolds number. The maximum average Darcy friction factor has been obtained at Case 1, whereas minimum one is at Case 12. Since Case 12 gives the highest heat transfer rate and lowest pressure loss, the best case is the Case 12 for the 100 twisting ratio pin fin condition (*TR*=100).

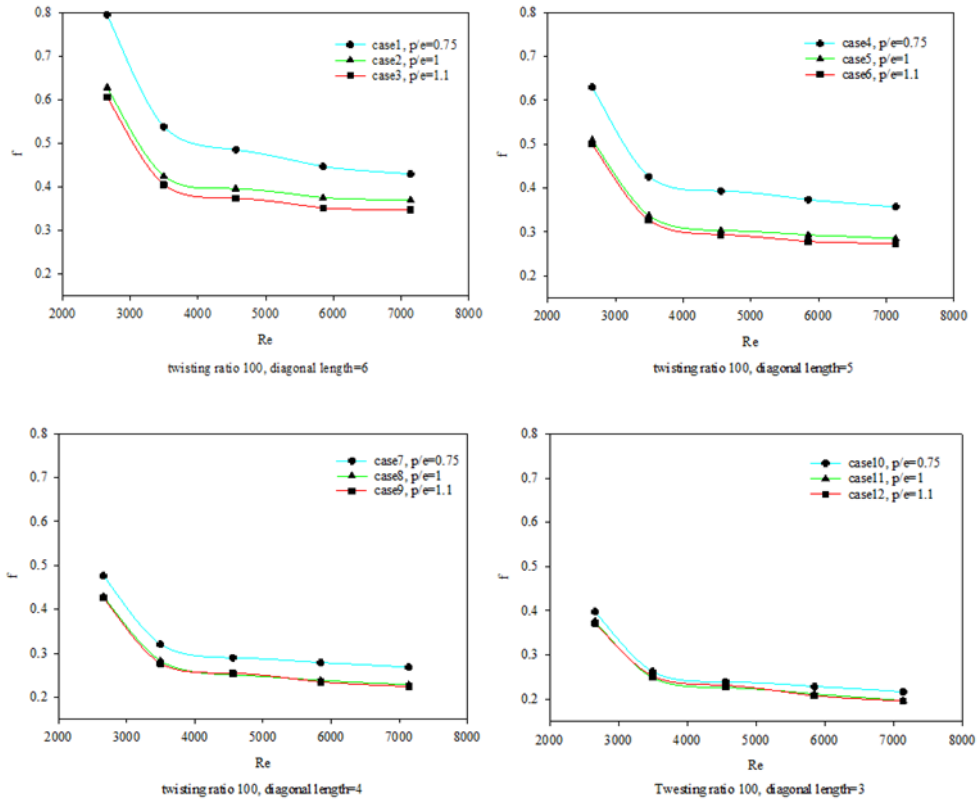

Figure 4.20. Average Darcy friction factor with Reynolds number in different diagonal lengths for *TR*=100.

Static temperature distribution over the heat sink is given in Figure 4.21 at *Re*=7138. Temperature magnitude on the heat sink is maximum in Case 1 and minimum in Case 12. It can also be said that the maximum effective cooling on heat sink is achieved in Case 12, whereas minimum is in Case 1. Less cooling is obtained over the heat sink at the wider diagonal length, while due to the increased interaction of the heat sink and coolant fluid the narrower diagonal length leads to greater cooling over the heat sink for all cases. That is the reason for obtaining more convective heat transfer rate.

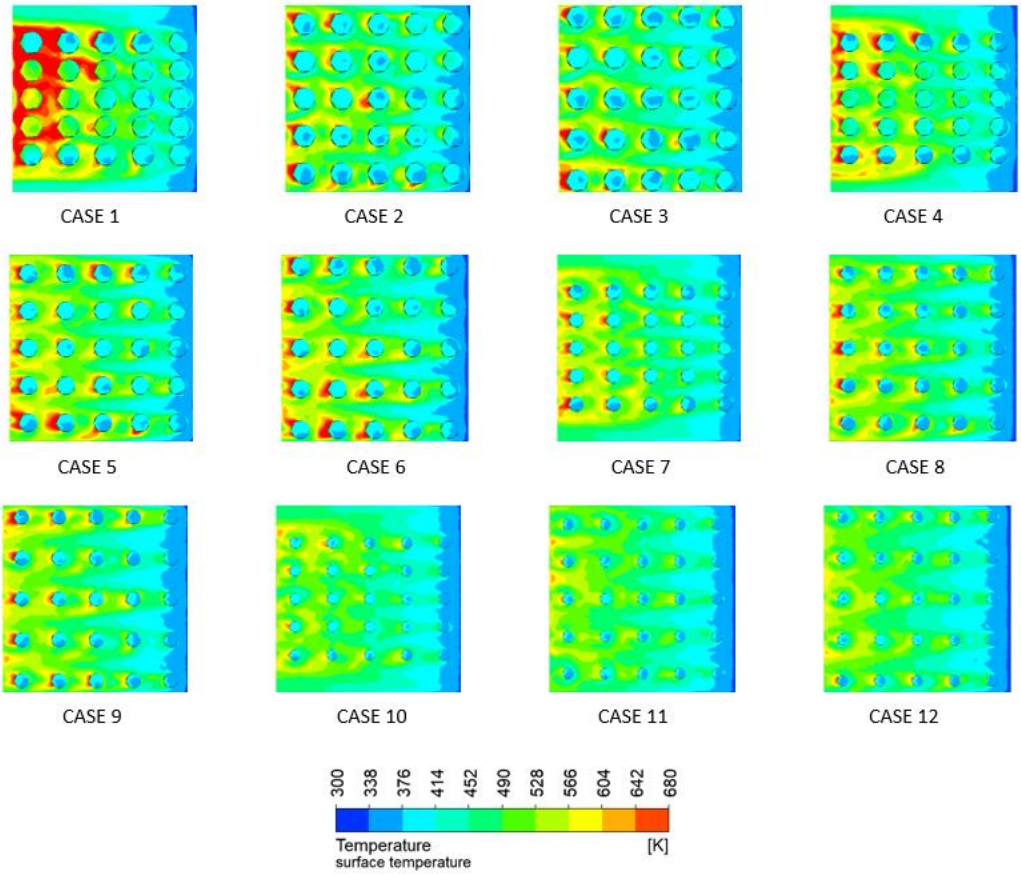

Figure 4.21. Static temperature distribution over the heat sink in different cases at *Re*=7138 with *TR*=100.

Variation of average heat transfer of heat sink is given in Figure 4.22. The average heat sink temperature in Case 12 is lower compared to the other cases, in despite of the wider pitch ratio of the pin fins and the lower diagonal length. Faster flow between the pin fins and the heat sink surface and higher heat transfer rate and lower average surface temperature for all Reynolds numbers are obtained when using a small diagonal length with a high pitch ratio. Whereas, the maximum average temperature of the heat sink is reached at the lowest Reynolds number, the minimum average temperature of the heat sink is obtained at the highest Reynolds numbers.

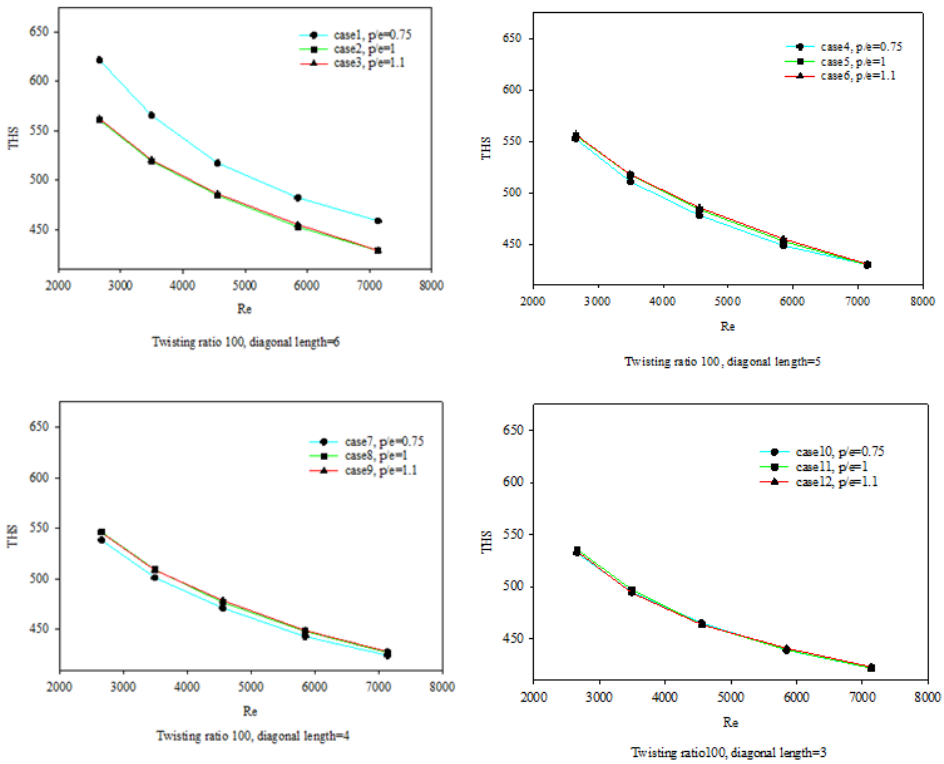

Figure 4.22. Variations of average temperature of heat sink for all cases for *TR*=100.

Thermal resistance is another important parameter of the heat sink applications. Variation of the thermal resistance with Reynolds number for different cases is given in Figure 4.23. The comparatively low average temperature of the heat sink gives the lower thermal resistance. So, lower thermal resistance is obtained in Case 12, and the higher one is in Case 1. Decreasing thermal resistance results in a positive effect on the performance of convective heat transfer.

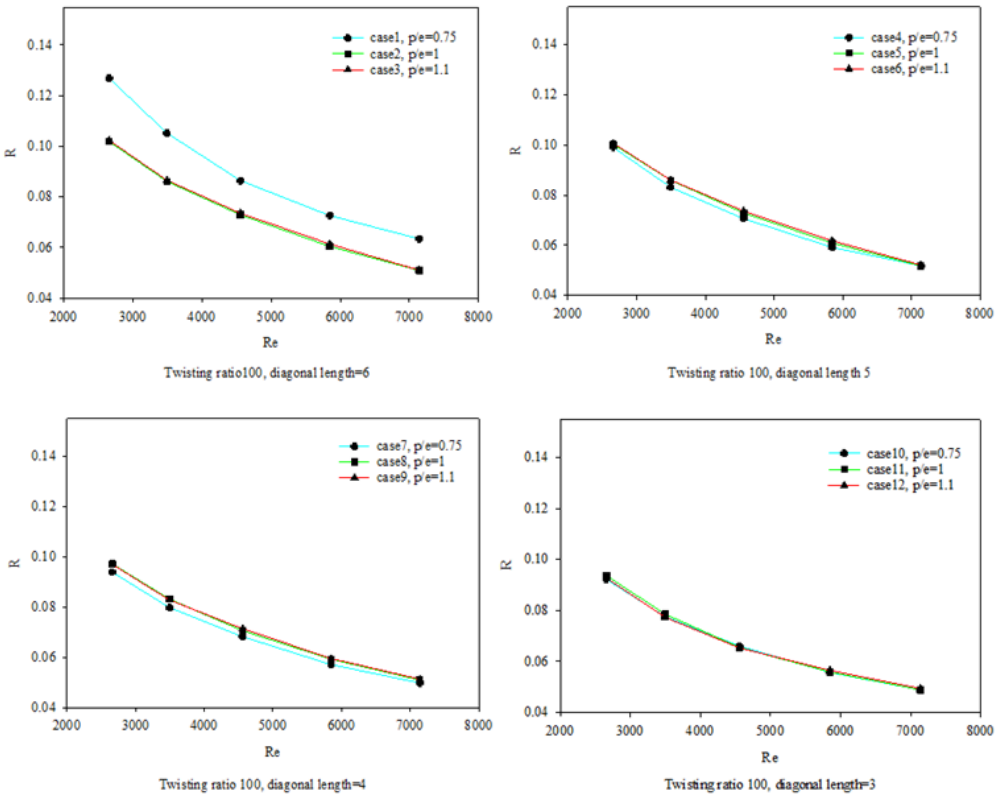

Figure 4.23. Thermal resistance with Reynolds number for all cases in *TR*=100.

The features of the vorticity distribution on the heat sink are presented in Figure 4.24 for different cases at *Re*=7138. The plane surface has been generated 5 mm from the surface of heat sink for taking the contour graph. The vorticity distribution has been taken on this plane surface. Strong vortices occurred on the upper and lower surfaces in the horizontal direction, and in the vertical direction at the beginning of the heat sink and the first column of pin fins due to the increase in fluid velocity. Due to the uniform distribution of fluid flow between the pin fins, a decrease in vorticity occurs when the diagonal length of the pin fins is reduced, and the pitch ratio increases. With an increase in the pitch ratio on the lower surface of the heat sink, the vortices are taken higher, and when the diagonal length decreases on the top surface of the pin, the vortices occur less. Heat transfer rate is enhanced by reducing radial length and increasing pitch ratio, results in the occurrence of more uniformity and stronger rotation over the heat sink.

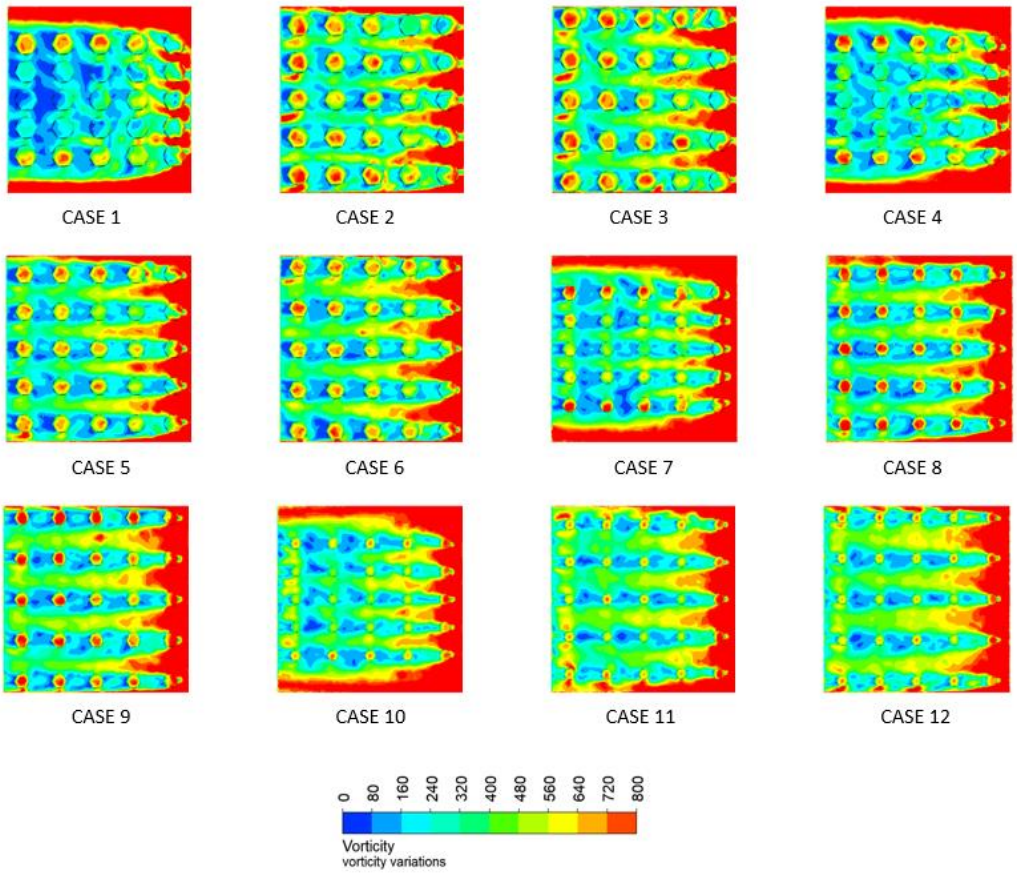

Figure 4.24. Vorticity variations over the heat sink in different cases at *Re*=7138 for *TR*=100.

Temperature streamlines on the generated plane surface at *Re*=7138 for different cases is given in Figure 4.25. As shown in Case 1 and Case 4, the velocity of the coolant is relatively high at the beginning of the heat sink, while it decreases with the movement of the fluid in the direction of the streamline due to the denser formation of the pin fins. More uniform streamline over the heat sink is achieved and so higher convective heat transfer rate with the decrease in diagonal length and increase in pitch ratio.

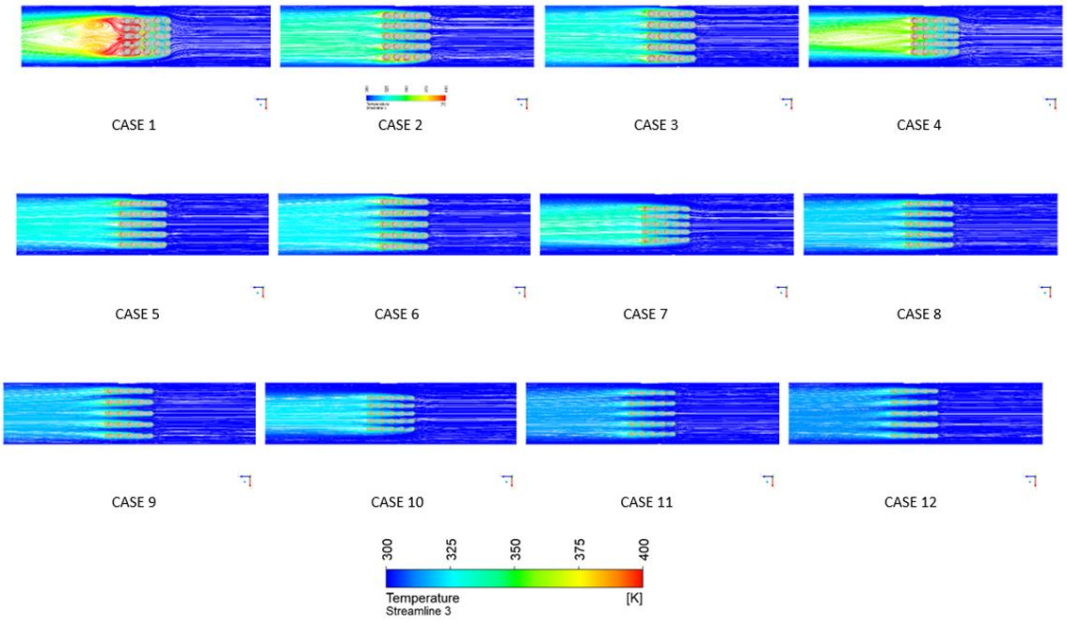

Figure 4.25. Temperature streamline toward streamwise direction for all cases at *Re*=7138 for *TR*=100.

Also, one of the important parameters is the *PEC* number which can be seen in Figure 4.26. For all the cases in different diagonal length noticing clearly that the PEC number decreases after Case 1 and stays almost stable for the rest of the cases. It is obtained that Case 1 is the most efficient case for the case of twisted pin fins with *TR*=200. It is also seen that twisting of the pin fin for other cases does not affect on the thermal performance since *PEC* numbers are almost unity.

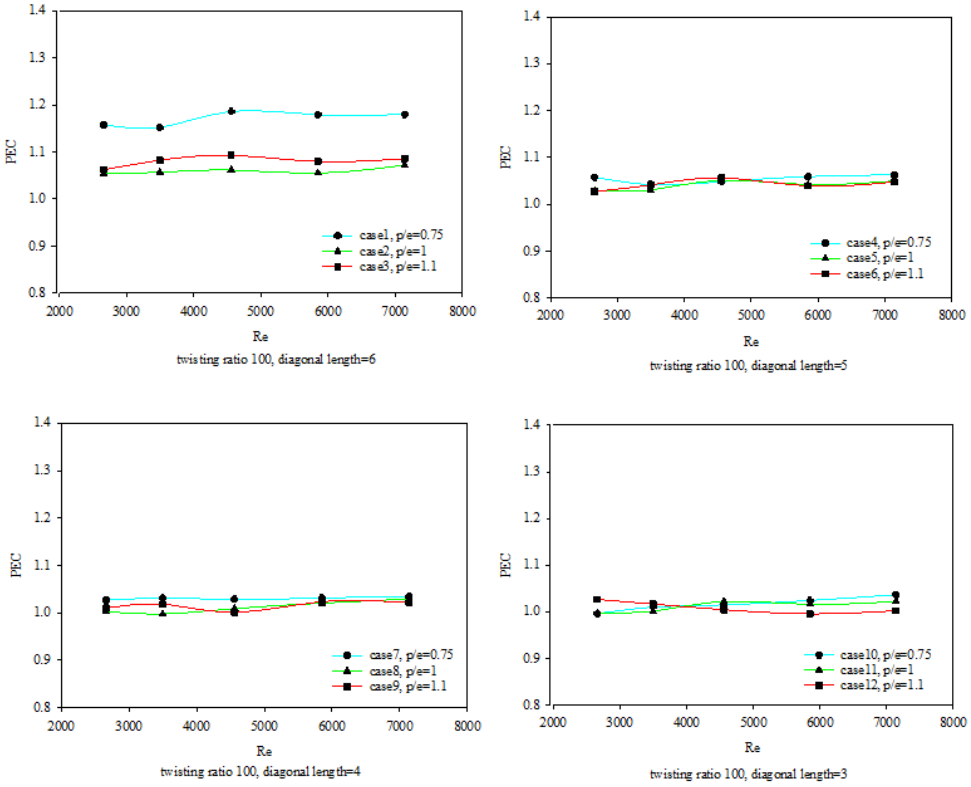

Figure 4.26. PEC number for all cases at *Re*=7138 with *TR*=100.

4.4. TWISTED PIN FINS WITH *TR*=50

In this case, calculation results for 50 twisting ratio pin fin condition (*TR*=50) are presented and discussed in detailed. Variations of average Nusselt number with Reynolds number are presented in Figure 4.27 for each case. It can be seen in this figure that average Nusselt number increases with increasing Reynolds number. the highest heat transfer rate is reached in Case 10, whereas lowest one is in Case 1 for all Reynolds numbers. It can also be obtained that decreasing diagonal length and increasing pitch ratio increase the heat transfer rate on the heat sink. The maximum average Nusselt number is determined as 101.834 for *Re*=7138.

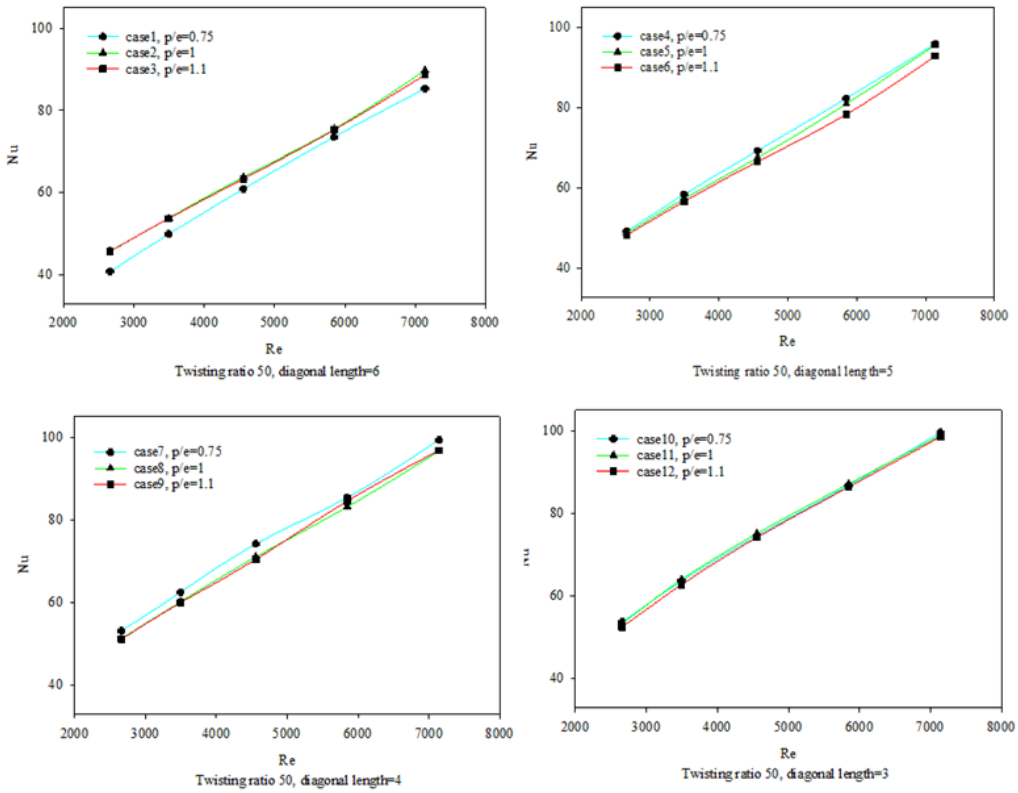

Figure 4.27. Average Nusselt number with Reynolds number in different cases for *TR*=50.

The surface Nusselt number distribution on the heat sink at *Re*=7138 for different cases can be seen in Figure 4.28. It is determined that reducing the diagonal length of the pin fin provides a more stable flow over the heat sink and it increases the surface Nusselt number. It can also be seen that the surface Nusselt number decreases in the streamwise direction.

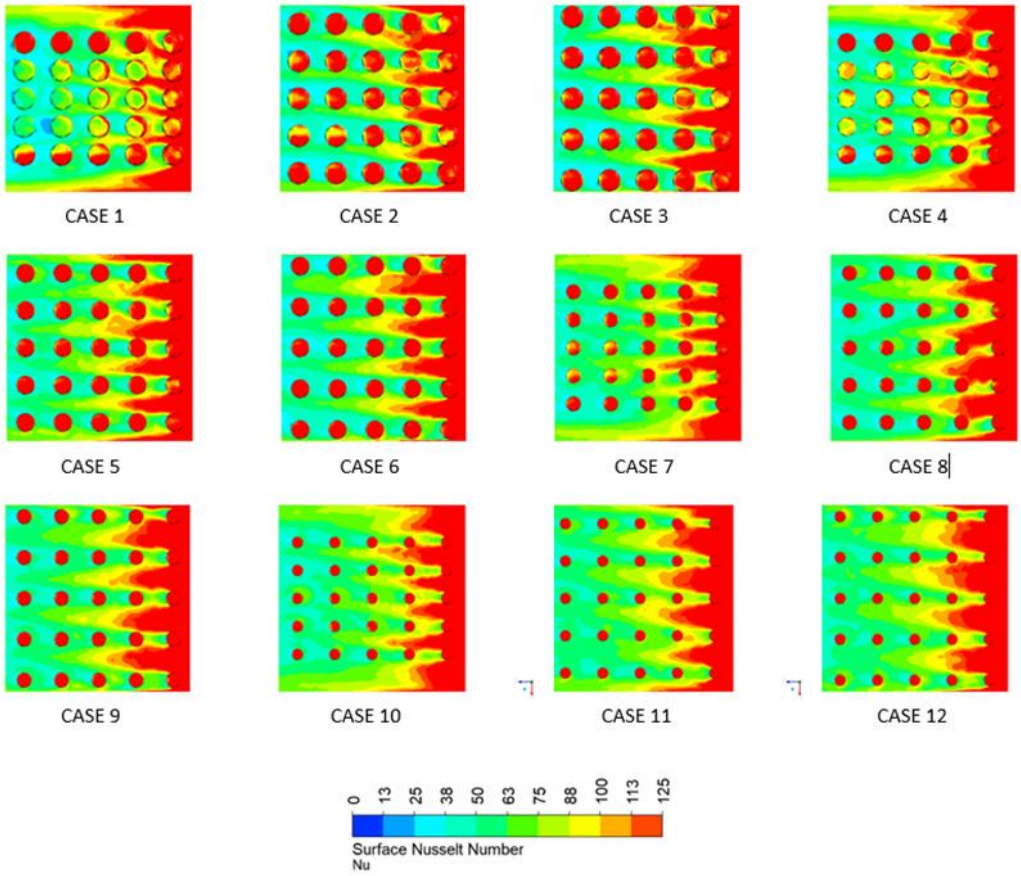

Figure 4.28. Surface Nusselt number distribution over the heat sink in different cases at *Re*=7138 for *TR*=50

Deciding the configuration is acceptable or not, it is important parameter to obtain the hydraulic performance of the novel heat sink design and it is also important in terms of research, innovation, and commercialization. To illustrate the hydraulic performance of the heat sink, variation of average Darcy friction factor with Reynolds number for different cases is presented in Figure 4.29. It can be revealed from the figure that average Darcy friction factor decreases with Reynolds number. The maximum average Darcy friction factor has been obtained at Case 1, whereas minimum one is at Case 12. Since Case 12 gives the highest heat transfer rate and lowest pressure loss, the best case is the Case 12 for *TR*=50.

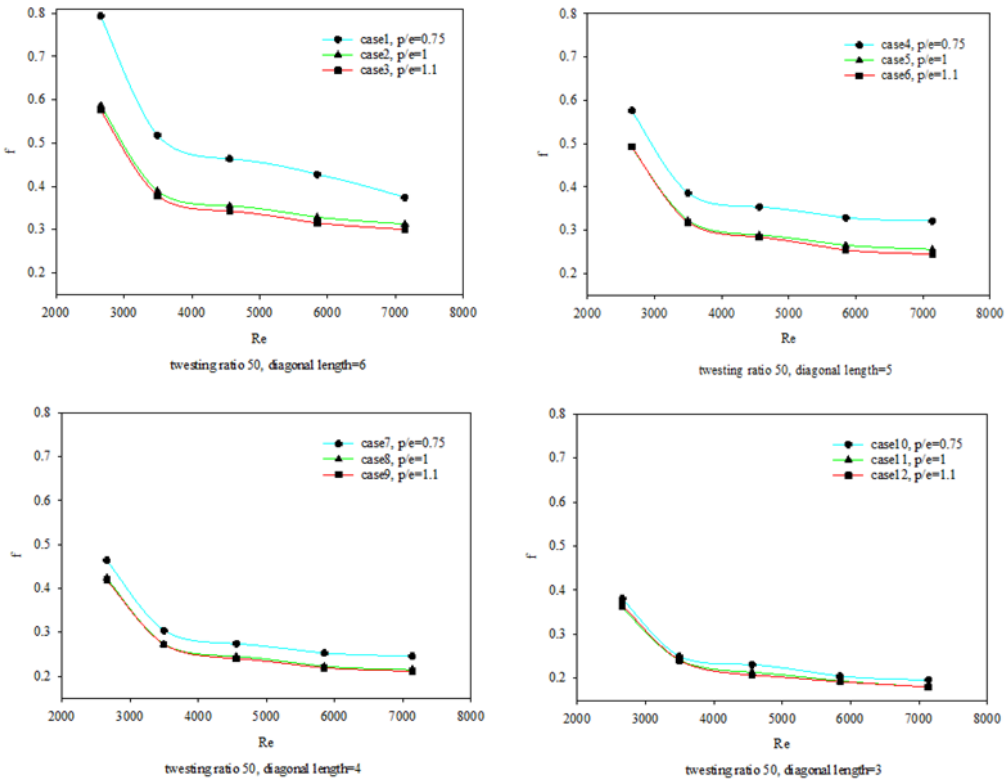

Figure 4.29. Average Darcy friction factor with Reynolds number in different cases for *TR*=50.

Static temperature distribution over the heat sink is given in Figure 4.30 at *Re*=7138. Temperature magnitude on the heat sink is maximum in Case 1 and minimum in Case 12. It can also be said that the maximum effective cooling on heat sink is achieved in Case 12, whereas minimum is in Case1. Less cooling is obtained over the heat sink at the wider diagonal length, while due to the increased interaction of the heat sink and coolant fluid the narrower diagonal length leads to greater cooling over the heat sink for all cases. That is the reason for obtaining more convective heat transfer rate.

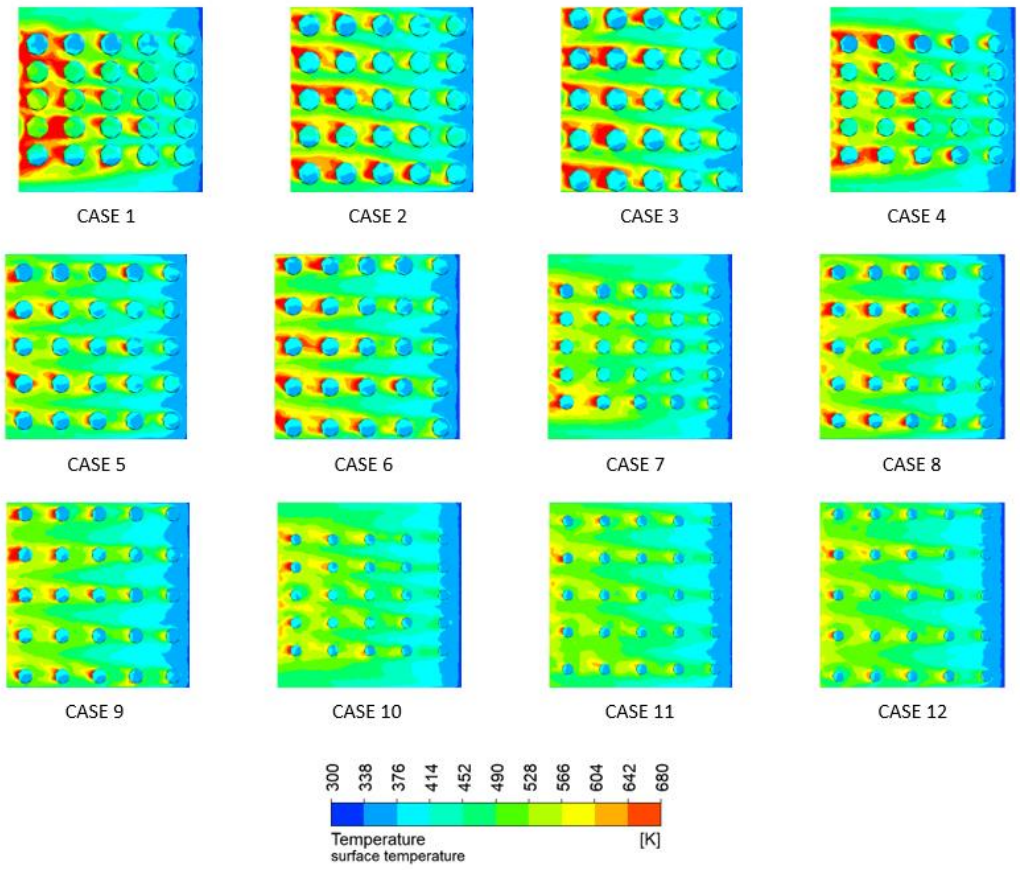

Figure 4.30. Static temperature distribution over the heat sink in different cases at *Re*=7138 for *TR*=50.

Variation of average heat transfer of heat sink is given in Figure 4.31. The average heat sink temperature in Case 12 is lower compared to the other cases, in despite of the wider pitch ratio of the pin fins and the lower diagonal length. Faster flow between the pin fins and the heat sink surface and higher heat transfer rate and lower average surface temperature for all Reynolds numbers are obtained when using a small diagonal length with a high pitch ratio. Whereas, the maximum average temperature of the heat sink is reached at the lowest Reynolds number, the minimum average temperature of the heat sink is obtained at the highest Reynolds numbers.

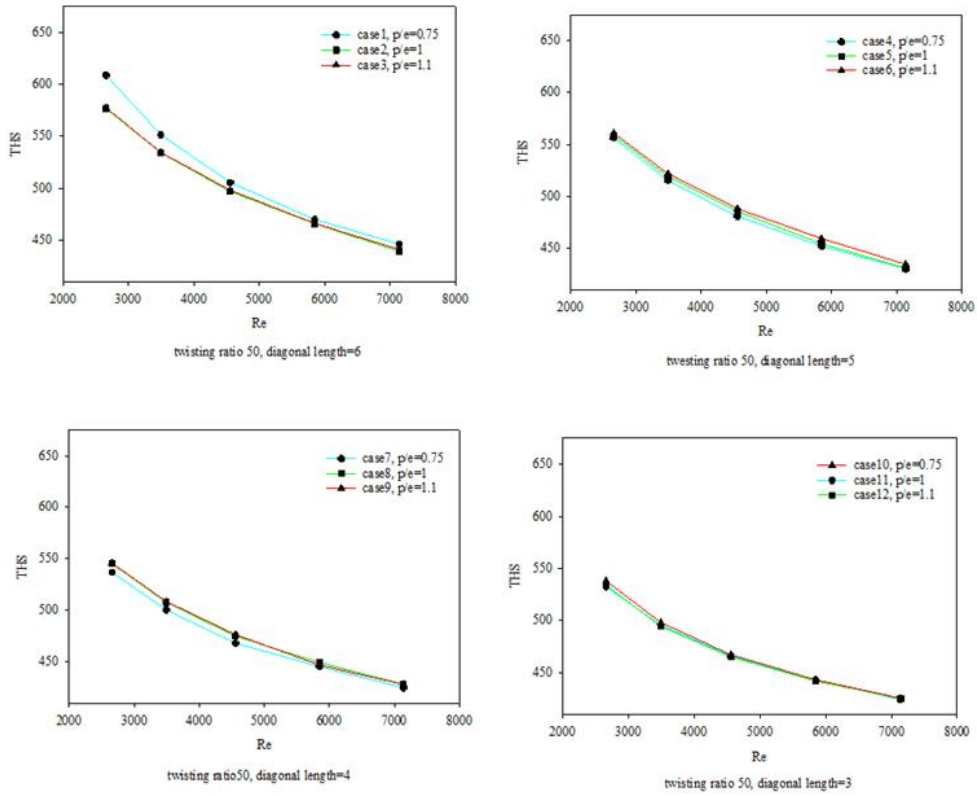

Figure 4.31. Variations of average temperature of heat sink for all cases for *TR*=50.

Thermal resistance is another important parameter of the heat sink applications. Variation of the thermal resistance with Reynolds number for different cases is given in Figure 4.32. The comparatively low average temperature of the heat sink gives the lower thermal resistance. So, lower thermal resistance is obtained in Case 12, and the higher one is in Case 1. Decreasing thermal resistance results in a positive effect on the performance of convective heat transfer.

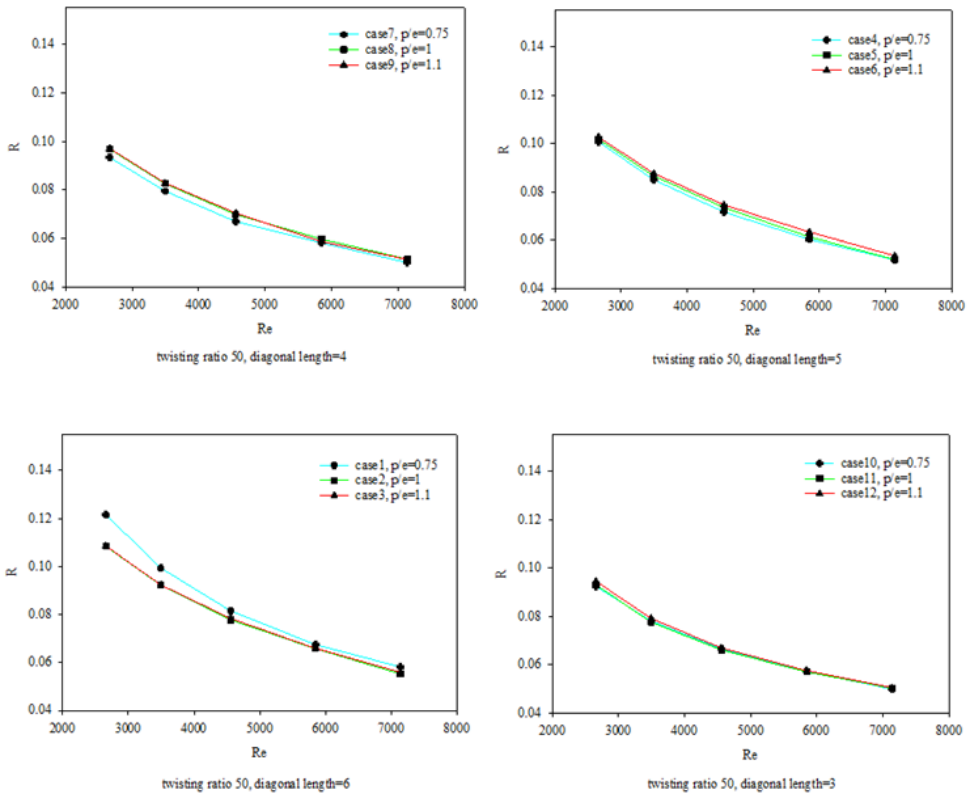

Figure 4.32. Thermal resistance with Reynolds number for all cases for *TR*=50.

The features of the vorticity distribution on the heat sink are presented in Figure 4.33 for different cases at *Re*=7138. The plane surface has been generated 5 mm from the surface of heat sink for taking the contour graph. The vorticity distribution has been taken on this plane surface. Strong vortices occurred on the upper and lower surfaces in the horizontal direction, and in the vertical direction at the beginning of the heat sink and the first column of pin fins due to the increase in fluid velocity. Due to the uniform distribution of fluid flow between the pin fins, a decrease in vorticity occurs when the diagonal length of the pin fins is reduced, and the pitch ratio increases. With an increase in the pitch ratio on the lower surface of the heat sink, the vortices are taken higher, and when the diagonal length decreases on the upper surface of the pin, the vortices occur less. Heat transfer rate is enhanced by reducing radial length and increasing pitch ratio, results in the occurrence of more uniformity and stronger rotation over the heat sink.

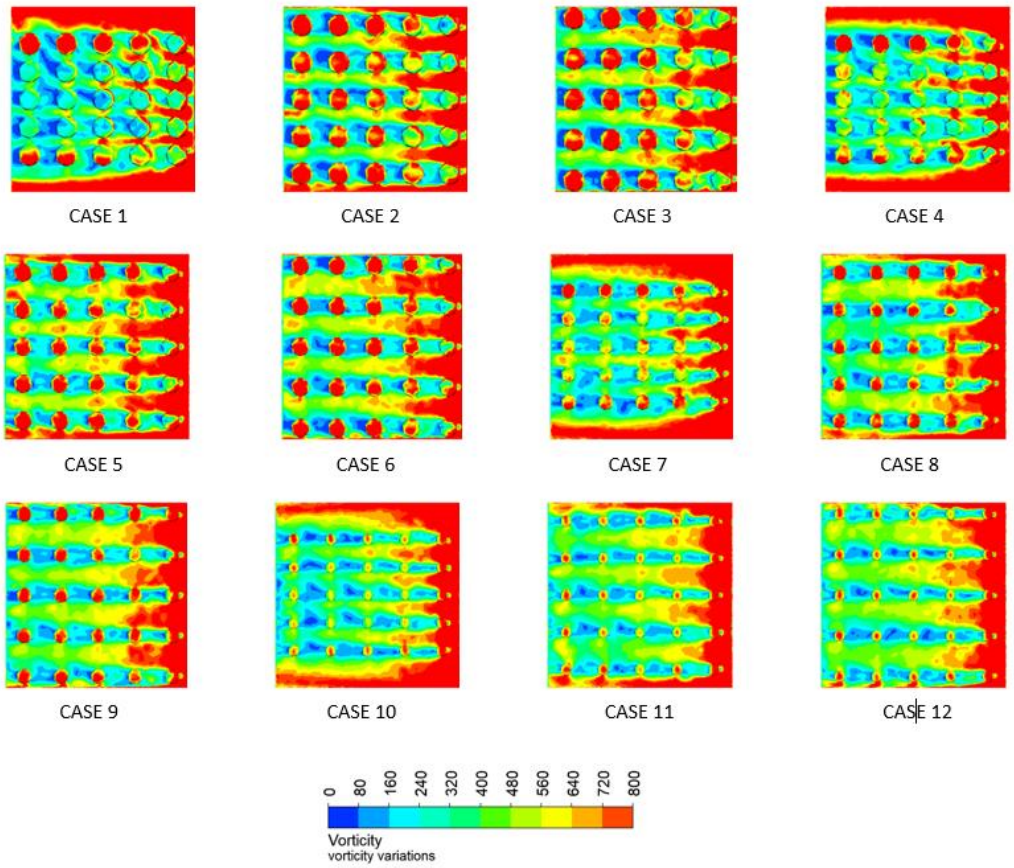

Figure 4.33. Vorticity variations over the heat sink in different cases at *Re*=7138 for *TR*=50.

Temperature streamlines on the generated plane surface at *Re*=7138 for different cases is given in Figure 4.34. As shown in Case 1 and Case 4, the velocity of the coolant is relatively high at the beginning of the heat sink, while it decreases with the movement of the fluid in the direction of the streamline due to the denser formation of the pin fins. More uniform streamline over the heat sink is achieved and so higher convective heat transfer rate with the decrease in diagonal length and increase in pitch ratio.

Also, one of the important parameters is the *PEC* number which can be seen in Figure 4.35. For all the cases in different diagonal length noticing clearly that the PEC number decreases after Case 1 and stays almost stable for the rest of the cases. It is obtained that Case 1 is the most efficient case for the case of twisted pin fins with *TR*=50. It is also seen that twisting of the pin fin for other cases does not effect on the thermal performance since *PEC* numbers are almost 1.

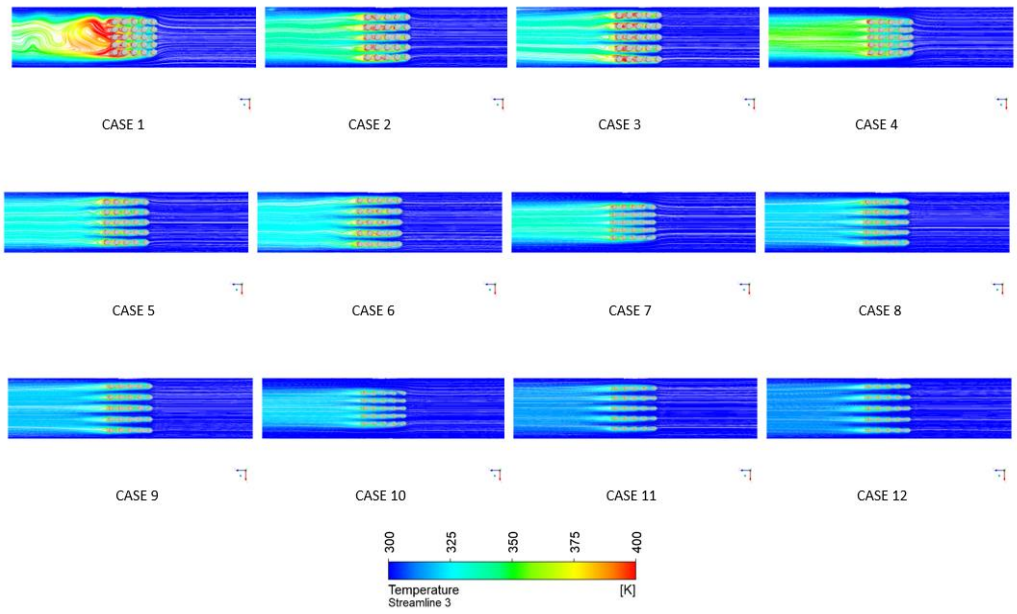

Figure 4.34. Temperature streamline toward streamwise direction for all cases at *Re*=7138 for *TR*=50.

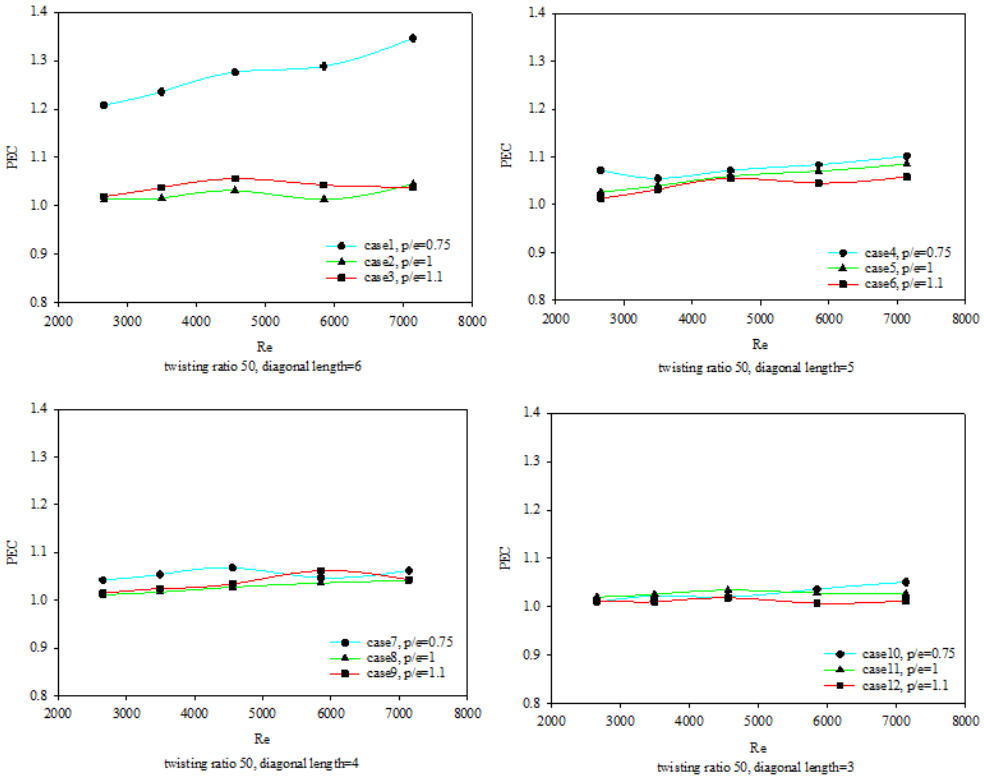

Figure 4.35. *PEC* number for all cases at *Re*=7138 for *TR*=50.

4.5. COMPARING PITCH RATIO FOR ALL THE CASES

As it has been mentioned before the main parameter that shows the efficiency of the design is the *PEC* number. Which represent the ratio of heat transfer rate to the ratio of pressure drop. All the values were taken at the same Reynolds number, diagonal length and pitch ratio due to considering the case with no twisting ratio or optimum case. Three different twisting ratios have been applied to the pin fins in our research in order to reach to the best design. The *PEC* number for all cases in each design has been compared in Figure 4.36 in order to get the best case for the study.

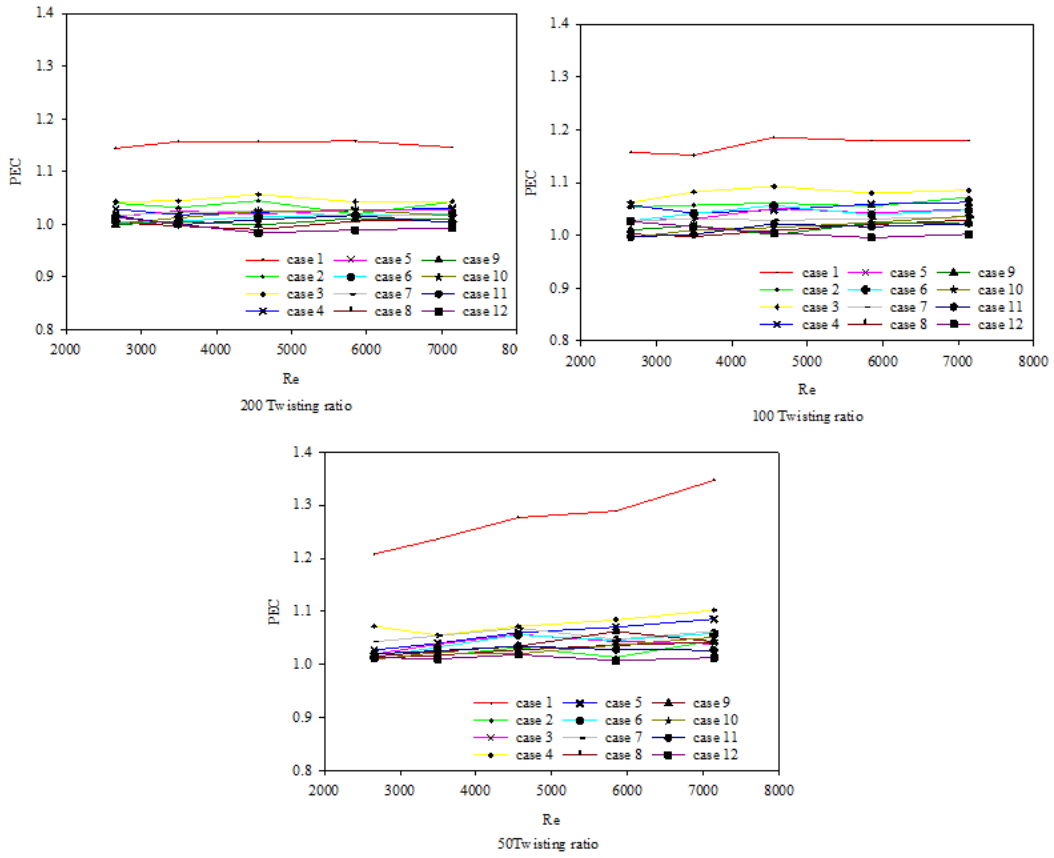

Figure 4.36. *PEC* numbers for all cases in each twisting ratio.

Comparing all cases, it was obtained that the best case is the Case 1 with highest diagonal length and lowest pitch ratio. The value of the pitch ratio is 0.75 and the diagonal length is 6 for Case 1 gives the highest *PEC* number.

The optimum cases for each design were taken and given in Figure 4.37. The highest *PEC* number has been obtained for *TR*=50 with the condition of L_{ef}=6 and *p/e*=0.75 at *Re*=7138. It was also obtained that reducing the twisting ratio with increasing pitch ratio and decreasing diagonal length give the higher heat transfer rates.

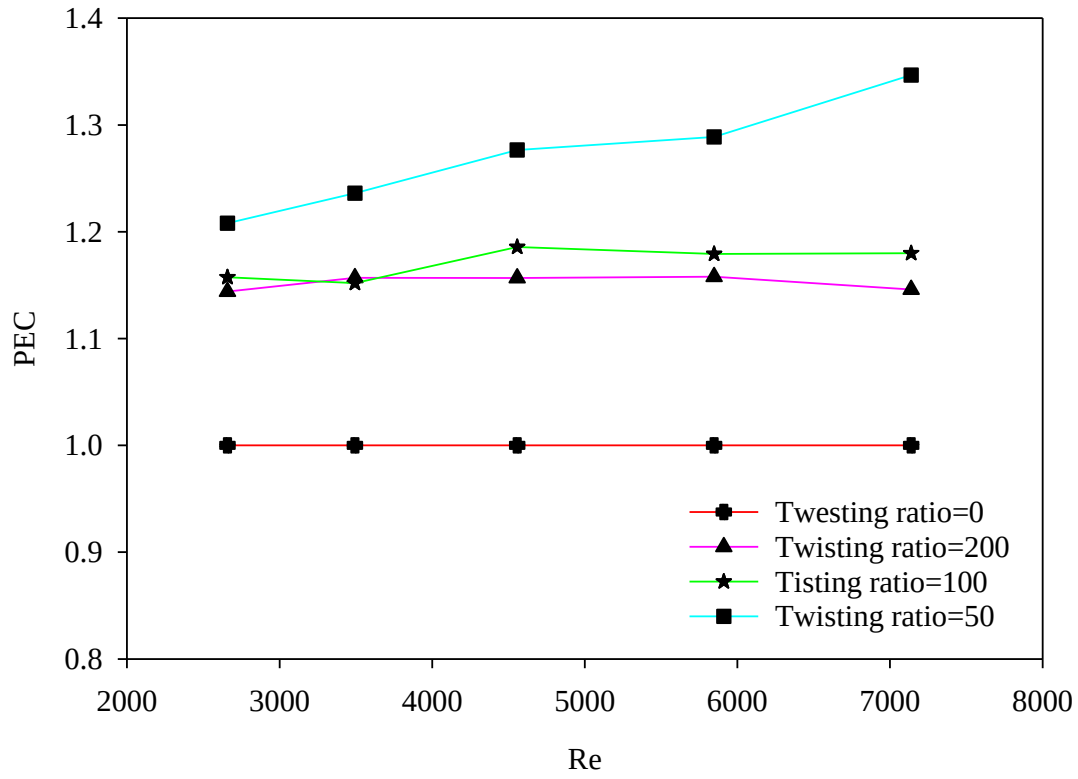

Figure 4.37. *PEC* numbers for the optimum case in each twisting value.

PART 5

CONCLUSION

In this study, the effects of pitch ratio and diagonal length of twisted pin fin array in heat sink on the flow and heat transfer characteristics have been determined numerically. Numerical calculations have been conducted under turbulent flow condition ($2658 \leq Re \leq 7138$). While the length of edge has been changed $3 \leq L_{ef} \leq 6$ and the pitch ratio has also been varied between $0.75 \leq p/e \leq 1.1$. Variation of twisting ratio (TR=50, 100, 200) of the pin fins has also been examined in detail.

The findings in this study are summarized below:

- Convective heat transfer rate for twisted and non-twisted fin increases with the increase in Reynolds number.
- The improvement of the convective heat transfer for the twisted pin fin is higher than the improvement in non-twisted pin fin for all twisting angles.
- Higher Nusselt numbers are obtained for the twisted fins than the non-twisted at all Reynolds numbers.
- Non-twisted pin fins have higher thermal resistance than the twisted pin fins. Also, thermal resistance decreases with decreasing Reynolds number.
- Pressure drops for the non-twisted pin fins arrays are higher than the twisted ones.
- More uniform temperature distribution and increment in convective heat transfer rate have been provided by decreasing in diagonal length, increasing in Reynolds number and pitch ratio.
- The most efficient case has been obtained for TR=50 with the condition of L_{ef}=6 and p/e=0.75 at Re=7138.

REFERENCES

1. El-Said, E. M. S., Abdelaziz, G. B., Sharshir, S. W., Elsheikh, A. H., and Elsaid, A. M., "Experimental investigation of the twist angle effects on thermo-hydraulic performance of a square and hexagonal pin fin array in forced convection", ***International Communications In Heat And Mass Transfer***, 126: 105374 (2021).

2. "Industry Developments: Heat Exchangers for Electronics Cooling | Advanced Thermal Solutions", **https://www.qats.com/cms/2017/05/25/industry-developments-heat-exchangers-for-electronics-cooling/** (2022).

3. Sahin, B., Yakut, K., Kotcioglu, I., and Celik, C., "Optimum design parameters of a heat exchanger", ***Applied Energy***, 82 (1): 90–106 (2005).

4. Gurrum, S. P., Suman, S. K., Joshi, Y. K., and Fedorov, A. G., "Thermal issues in next-generation integrated circuits", ***IEEE Transactions On Device And Materials Reliability***, 4 (4): 709–714 (2004).

5. Park, K., Choi, D. H., and Lee, K. S., "NUMERICAL SHAPE OPTIMIZATION FOR HIGH PERFORMANCE OF A HEAT SINK WITH PIN-FINS", ***Http://Dx.Doi.Org/10.1080/104077890503934***, 46 (9): 909–927 (2010).

6. Caputo, A. C., Pelagagge, P. M., and Salini, P., "Heat exchanger design based on economic optimisation", ***Applied Thermal Engineering***, 28 (10): 1151–1159 (2008).

7. Greenberg, S., Mills, E., Tschudi, B., Berkeley, L., Laboratory, N., Rumsey, P., Engineers, R., and Myatt, B., "Best Practices for Data Centers: Lessons Learned from Benchmarking 22 Data Centers The Data Center Challenge", (2006).

8. Edreis, E. and Petrov, A., "Types of heat exchangers in industry, their advantages and disadvantages, and the study of their parameters", ***IOP Conference Series: Materials Science And Engineering***, 963 (1): 012027 (2020).

9. Hanshik, C., Jeong, H., Jeong, K. W., and Choi, S. H., "Improved productivity of the MSF (multi-stage flashing) desalination plant by increasing the TBT (top brine temperature)", ***Energy***, 107: 683–692 (2016).

10. "Heat Transfer by Shell and Tube Heat Exchangers", **https://www.wermac.org/equipment/heatexchanger_part2.html** (2022).

11. "Overview of Plate Heat Exchanger with Steam (PDF) – What Is Piping", **https://whatispiping.com/plate-heat-exchanger-with-steam-1/** (2022).

12. Kistler, R. S. and Chenoweth, J. W., "Heat exchanger shellside pressure drop: Comparison of predictions with experimental data", ***Journal Of Heat Transfer***, 110 (1): 68–76 (1988).

13. "Effective Cooling with ATS Heat Sinks | Electronic Components. Distributor, Online Shop – Transfer Multisort Elektronik", **https://www.tme.eu/en/news/library-articles/page/43134/effective-cooling-with-ats-heat-sinks/** (2022).

14. Khan, J., Momin, S. A., and Mariatti, M., "A review on advanced carbon-based thermal interface materials for electronic devices", ***Carbon***, 168: 65–112 (2020).

15. Dai, J., Ohadi, M. M., Das, D., and Pecht, M. G., "Optimum cooling of data centers: Application of risk assessment and mitigation techniques", ***Optimum Cooling Of Data Centers: Application Of Risk Assessment And Mitigation Techniques***, 1–186 (2014).

16. Shahsavar, A., Shahmohammadi, M., and Baniasad Askari, I., "The effect of inlet/outlet number and arrangement on hydrothermal behavior and entropy generation of the laminar water flow in a pin-fin heat sink", ***International Communications In Heat And Mass Transfer***, 127: 105500 (2021).

17. Sidik, N. A. C., Muhamad, M. N. A. W., Japar, W. M. A. A., and Rasid, Z. A., "An overview of passive techniques for heat transfer augmentation in microchannel heat sink", ***International Communications In Heat And Mass Transfer***, 88: 74–83 (2017).

18. Alomar, O. R., Yousif, Q. A., and Mohamed, I. A., "Numerical Simulation of Natural Convection and Radiation on Performance of uniform Fins Geometry", ***2019 International Conference On Advanced Science And Engineering, ICOASE 2019***, 208–213 (2019).

19. Turkyilmazoglu, M., "Efficiency of heat and mass transfer in fully wet porous fins: Exponential fins versus straight fins", ***International Journal Of Refrigeration***, 46: 158–164 (2014).

20. Turkyilmazoglu, M., "Stretching/shrinking longitudinal fins of rectangular profile and heat transfer", ***Energy Conversion And Management***, 91: 199–203 (2015).

21. Turkyilmazoglu, M., "Heat transfer from moving exponential fins exposed to heat generation", ***International Journal Of Heat And Mass Transfer***, 116: 346–351 (2018).

22. Ghani, I. A., Kamaruzaman, N., and Sidik, N. A. C., "Heat transfer augmentation in a microchannel heat sink with sinusoidal cavities and rectangular ribs", ***International Journal Of Heat And Mass Transfer***, 108: 1969–1981 (2017).

23. Mousavi, H., Rabienataj Darzi, A. A., Farhadi, M., and Omidi, M., "A novel heat sink design with interrupted, staggered and capped fins", ***International Journal Of Thermal Sciences***, 127: 312–320 (2018).

24. Jajja, S. A., Ali, W., Ali, H. M., and Ali, A. M., "Water cooled minichannel heat sinks for microprocessor cooling: Effect of fin spacing", ***Applied Thermal Engineering***, 64 (1–2): 76–82 (2014).

25. Patel, N. and Mehta, H. B., "Experimental investigations on a variable channel width double layered minichannel heat sink", ***International Journal Of Heat And Mass Transfer***, 165: 120633 (2021).

26. Yan, Y., He, Z., Wu, G., Zhang, L., Yang, Z., and Li, L., "Influence of hydrogels embedding positions on automatic adaptive cooling of hot spot in fractal microchannel heat sink", ***International Journal Of Thermal Sciences***, 155: 106428 (2020).

27. Lin, L., Zhao, J., Lu, G., Wang, X. D., and Yan, W. M., "Heat transfer enhancement in microchannel heat sink by wavy channel with changing wavelength/amplitude", ***International Journal Of Thermal Sciences***, 118: 423–434 (2017).

28. Ermagan, H. and Rafee, R., "Numerical investigation into the thermo-fluid performance of wavy microchannels with superhydrophobic walls", ***International Journal Of Thermal Sciences***, 132: 578–588 (2018).

29. Ren, Q., Wang, Z., Zhu, J., and Qu, Z. G., "Pore-scale heat transfer of heat sink filled with stacked 2D metal fiber-PCM composite", ***International Journal Of Thermal Sciences***, 161: 106739 (2021).

30. Chiam, Z. L., Lee, P. S., Singh, P. K., and Mou, N., "Investigation of fluid flow and heat transfer in wavy micro-channels with alternating secondary branches", ***International Journal Of Heat And Mass Transfer***, 101: 1316–1330 (2016).

31. Izadi, M., Sheremet, M. A., Mehryan, S. A. M., Pop, I., Öztop, H. F., and Abu-Hamdeh, N., "MHD thermogravitational convection and thermal radiation of a micropolar nanoliquid in a porous chamber", ***International Communications In Heat And Mass Transfer***, 110: 104409 (2020).

32. Izadi, M., Mohammadi, S. A., Mehryan, S. A. M., Yang, T. F., and Sheremet, M. A., "Thermogravitational convection of magnetic micropolar nanofluid with coupling between energy and angular momentum equations", ***International Journal Of Heat And Mass Transfer***, 145: 118748 (2019).

33. Izadi, M., Hashemi Pour, S. M. R., Karimdoost Yasuri, A., and Chamkha, A. J., "Mixed convection of a nanofluid in a three-dimensional channel: Effect of opposed buoyancy force on hydrodynamic parameters, thermal parameters and entropy generation", ***Journal Of Thermal Analysis And Calorimetry***, 136 (6): 2461–2475 (2019).

34. Izadi, M., Javanahram, M., Zadeh, S. M. H., and Jing, D., "Hydrodynamic and heat transfer properties of magnetic fluid in porous medium considering nanoparticle shapes and magnetic field-dependent viscosity", ***Chinese Journal Of Chemical Engineering***, 28 (2): 329–339 (2020).

35. Izadi, M., Sheremet, M. A., and Mehryan, S. A. M., "Natural convection of a hybrid nanofluid affected by an inclined periodic magnetic field within a porous medium", ***Chinese Journal Of Physics***, 65: 447–458 (2020).

36. Izadi, M., "Effects of porous material on transient natural convection heat transfer of nano-fluids inside a triangular chamber", ***Chinese Journal Of Chemical Engineering***, 28 (5): 1203–1213 (2020).

37. Izadi, M., Ghalambaz, M., and Mehryan, S. A. M., "Location impact of a pair of magnetic sources on melting of a magneto-Ferro phase change substance", ***Chinese Journal Of Physics***, 65: 377–388 (2020).

38. Shahsavar, A., Jafari, M., Talebizadehsardari, P., and Toghraie, D., "Hydrothermal and entropy generation specifications of a hybrid ferronanofluid in microchannel heat sink embedded in CPUs", ***Chinese Journal Of Chemical Engineering***, 32: 27–38 (2021).

39. Shahsavar, A., Entezari, S., Toghraie, D., and Barnoon, P., "Effects of the porous medium and water-silver biological nanofluid on the performance of a newly designed heat sink by using first and second laws of thermodynamics", ***Chinese Journal Of Chemical Engineering***, 28 (11): 2928–2937 (2020).

40. Yoon, Y., Park, S. J., Kim, D. R., and Lee, K. S., "Thermal performance improvement based on the partial heating position of a heat sink", ***International Journal Of Heat And Mass Transfer***, 124: 752–760 (2018).

41. Ali, H. M., Arshad, A., Jabbal, M., and Verdin, P. G., "Thermal management of electronics devices with PCMs filled pin-fin heat sinks: A comparison", ***International Journal Of Heat And Mass Transfer***, 117: 1199–1204 (2018).

42. Deshmukh, P. A. and Warkhedkar, R. M., "Thermal performance of elliptical pin fin heat sink under combined natural and forced convection", ***Experimental Thermal And Fluid Science***, 50: 61–68 (2013).

43. Sangtarash, F. and Shokuhmand, H., "Experimental and numerical investigation of the heat transfer augmentation and pressure drop in simple, dimpled and perforated dimpled louver fin banks with an in-line or staggered arrangement", ***Applied Thermal Engineering***, 82: 194–205 (2015).

44. Bezaatpour, M. and Goharkhah, M., "Effect of magnetic field on the hydrodynamic and heat transfer of magnetite ferrofluid flow in a porous fin heat sink", ***Journal Of Magnetism And Magnetic Materials***, 476: 506–515 (2019).

45. Kabakuş, A., Yakut, K., Özakın, A. N., and Yakut, R., "Experimental determination of cooling performance on heat sinks with cone-jet electrospray mode", ***Engineering Science And Technology, An International Journal***, 24 (3): 665–670 (2021).

46. Bhandari, P. and Prajapati, Y. K., "Thermal performance of open microchannel heat sink with variable pin fin height", ***International Journal Of Thermal Sciences***, 159: 106609 (2021).

47. Ong, K. S., Tan, C. F., Lai, K. C., and Tan, K. H., "Heat spreading and heat transfer coefficient with fin heat sink", ***Applied Thermal Engineering***, 112: 1638–1647 (2017).

48. Ozsipahi, M., Subasi, A., Gunes, H., and Sahin, B., "Numerical investigation of hydraulic and thermal performance of a honeycomb heat sink", ***International Journal Of Thermal Sciences***, 134: 500–506 (2018).

49. Huang, C. H. and Chen, M. H., "An estimation of the optimum shape and perforation diameters for pin fin arrays", ***International Journal Of Heat And Mass Transfer***, 131: 72–84 (2019).

50. Soleymani, Z., Rahimi, M., Gorzin, M., and Pahamli, Y., "Performance analysis of hotspot using geometrical and operational parameters of a microchannel pin-fin hybrid heat sink", ***International Journal Of Heat And Mass Transfer***, 159: 120141 (2020).

51. Wang, S.-L., Chen, L.-Y., Zhang, B.-X., Yang, Y.-R., and Wang, X.-D., "A new design of double-layered microchannel heat sinks with wavy microchannels and porous-ribs", 141: 547–558 (2020).

52. Attar, M. R., Mohammadi, M., Taheri, A., Hosseinpour, S., Passandideh-Fard, M., Haddad Sabzevar, M., and Davoodi, A., "Heat transfer enhancement of conventional aluminum heat sinks with an innovative, cost-effective, and simple chemical roughening method", ***Thermal Science And Engineering Progress***, 20: 100742 (2020).

53. Tariq, A., Altaf, K., Ahmad, S. W., Hussain, G., and Ratlamwala, T. A. H., "Comparative numerical and experimental analysis of thermal and hydraulic performance of improved plate fin heat sinks", ***Applied Thermal Engineering***, 182: 115949 (2021).